R-09-41

Creep properties of phosphorus alloyed oxygen free copper under multiaxial stress state

Rui Wu, Facredin Seitisleam
Swerea KIMAB

Rolf Sandström, Swerea KIMAB,
Dept. of Materials Science and Engineering, KTH

October 2009

Svensk Kärnbränslehantering AB
Swedish Nuclear Fuel
and Waste Management Co

Box 250, SE-101 24 Stockholm
Phone +46 8 459 84 00

ISSN 1402-3091
SKB Rapport R-09-41

Creep properties of phosphorus alloyed oxygen free copper under multiaxial stress state

Rui Wu, Facredin Seitisleam
Swerea KIMAB

Rolf Sandström, Swerea KIMAB,
Dept. of Materials Science and Engineering, KTH

October 2009

Keywords: Phosphorus alloyed oxygen free copper canister, Creep, Notch, Notch strengthening, Multiaxial stress state, FEM-modelling.

Abstract

Phosphorus alloyed oxygen free copper (Cu-OFP) canisters are planned to be used for spent nuclear fuel in Sweden. The copper canisters will be subjected to creep under multiaxial stress states in the repository. Creep tests have therefore been carried out at 75°C using double notch specimens with notch acuities of 0.5, 2, 5, and 18.8, respectively. The creep lifetime for notched specimens is considerably longer than that for the smooth one at a given net section stress, indicating that the investigated Cu-OFP is notch insensitive (notch strengthening). The notch strengthening factor in time is, for instance, greater than 70 at 180 MPa for the bluntest notch (notch acuity = 0.5). The creep lifetime is notch acuity dependent. The sharper the notch, the longer the creep lifetime is. The creep deformation is to a significant extent concentrated to the region around the notches. Different deformation on the two notches is observed. Both axial and radial strains on the failed notch are several times larger than those on the unbroken one. Linear relation between the axial and the radial strains on the notches is found. Transgranular failure is predominant, independent of stress, rupture time, and notch acuity. Adjacent to fracture, elongated grains along the stress direction, separate pores and cavities are often visible. On the unbroken notch, fewer separate cavities and cracks are only seen intergranularly for the sharper notches (notch acuity ≥ 2).

To interpret the tests for the notched creep specimens, finite element computations have been performed. A fundamental model for primary and secondary creep without fitting parameters has been used as constitutive equation. The FEM-modelling could represent the creep strain versus time curves for the notched specimens in a satisfactory way. In these curves the strain on loading is included. From the FEM-computations a stationary creep stress could be assessed, which is close to the reference stress. For a given stationary creep stress, the rupture time can be estimated from the corresponding uniaxial data. This relation can be used to estimate the rupture time for components exposed to creep.

Contents

1 Introduction

Phosphorus alloyed oxygen free copper (Cu-OFP) copper canisters are planned to be used for spent nuclear fuel in the Swedish nuclear waste programme. In the repository the copper material will be deformed by creep at temperatures up to about 100°C. To ensure the integrity of the canisters against creep deformation, the copper material must have at least 10% creep ductility under the stress states that appear at critical positions. So far, uniaxial creep testing at Swerea KIMAB has been performed at various temperatures. However, the canister will be exposed to multiaxial stress states when the external hydrostatic pressure as well as the swelling pressure from the bentonite are developed.

Failure mechanisms, failure modes and fracture strain (ductility) are found to be affected by the stress state /1/–/4/. Components under a high state of multiaxial stress can fail prematurely due to the inhibition of deformation and enhancement in fracture processes /1/.

One established and convenient method of introducing a state of multiaxial stress into laboratory specimens is to subject circumferentially notched bars to an axial tensile stress /5/. Such notched bar specimens are relatively inexpensive to manufacture and can be tested in the same machine used to collect standard uniaxial data. In addition, various states of stress in terms of ratio between maximum principal stress and effective stress can be obtained and simulated by changing the notch profile /6/.

With the help of FEM-modelling, the creep deformation of the specimens can be simulated. In this way the role of the multiaxial stresses can be analysed, and the results can be generalised to other components.

In design when cracks are encountered, the simplest way is to estimate the average stress on the remaining section, the net section stress, and compare it with the design stress. A more sophisticated procedure is to use elastic-plastic FEM-modelling assuming a perfectly plastic material, yielding at different artificial stress levels. The minimum yielding stress (effective stress) that can support the external load, the reference stress, can be compared with the design stress. A still more advanced approach is to include a creep calculation in the FEM-model. The resulting (stationary effective) creep stresses can be related to the design stress. In the present paper all three methods will be analysed for notched specimens.

By using notched bar creep specimens, the other purposes of the present project are to study the creep lifetime and ductility of OFP-copper under multiaxial stress state, to compare creep behaviour under multiaxial stress state with that under uniaxial stress state, and to examine creep damage development.

2 Material and experiments

2.1 Material

A forged lid in as-hot worked soft condition made of pure, oxygen-free copper doped with about 50 ppm phosphorus (Cu-OFP) is used in this study. The lid is provided by Svensk Kärnbränslehantering AB (Swedish Nuclear Fuel and Waste Management Company, SKB). Plane cylindrical creep specimens for uniaxial testing were taken from this lid as well /7/. Chemical composition and mechanical properties of the material are given in /8/.

Mixed grain size is observed in the forged lid, see Figure 2-1. The grain size is also different at different positions of the lid. The average grain sizes adjacent to the centre and to the outside are 85 µm and 156 µm, respectively, see also Figure 2-1. The hardness (HV2), which is a mean value of three measurements, is 78.

2.2 Creep specimen

Extraction of the cylindrical, double notched creep specimens is attempted to keep a similar position as for the plane creep specimens in the lid. Two notches are introduced on a cylindrical creep specimen with threaded ends having a diameter of 8 mm in the gauge length and a total gauge length of about 51 mm, see Figure 2-2. The introduction of the notches will create a multiaxial stress state at the notches when subjected to tensile load. The fracture is expected to take place in one of the two notches, while the other unbroken one should represent the circumstances close to rupture, facilitating the creep damage investigation.

Four different notch acuities are chosen. The notch acuity, a/R, is set to be equal to 0.5, 2, 5 and 18.8, respectively. The parameter a is the radius of the specimen at the base of the notch position, and R the notch root radius. As an example, the cylindrical, double notched creep specimen with a notch acuity $a/R = 0.5$ is shown in Figure 2. According to the definition of the notch acuity a/R, the larger the a/R value, the sharper the notch.

The ratio of b/a is set to $\sqrt{2}$. The parameter b is the gross radius of the specimen, see also Figure 2-2. The dimension of the specimen corresponds to that recommended in the code of practice for notched bar testing /5/.

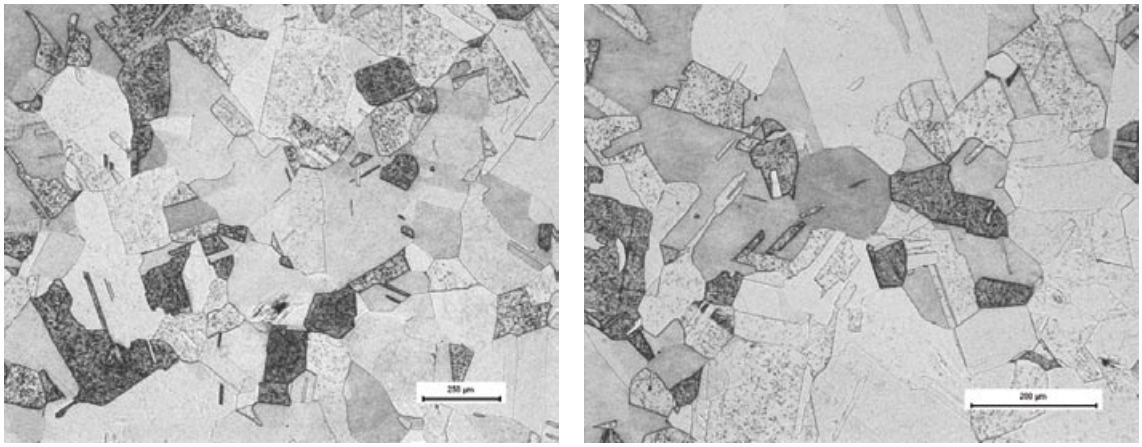

(a) (b)

Figure 2-1. *Grain size distribution in the forged lid (noting different scales). (a) Adjacent to the centre and (b) adjacent to the outside.*

2.3 Creep testing

By using single specimen, constant dead load creep testing machines the cylindrical, double notched creep specimens are isothermally tested at constant temperature of 75°C at different initial net section stresses, see Table 3-1. The net section stress is the applied axial load divided by the minimum cross section at the notch. Uniaxial load is axially applied on the specimens with measurement of the displacement over the whole gauge length. The tests are allowed to run to rupture. The tests may however be interrupted if an unreasonable long test duration appears.

2.4 Post test metallography

After creep testing, the failed specimens are longitudinally sectioned in the middle, mounted, ground and polished to 0.25 µm, and finally etched in a solution containing 40 g CrO_3, 7.5 g HN_4Cl, 50 ml H_2SO_4, 50 ml HNO_3 and 1,900 ml H_2O. Creep cavitation investigation is then carried out on the etched metallographic samples using light optical microscope (LOM).

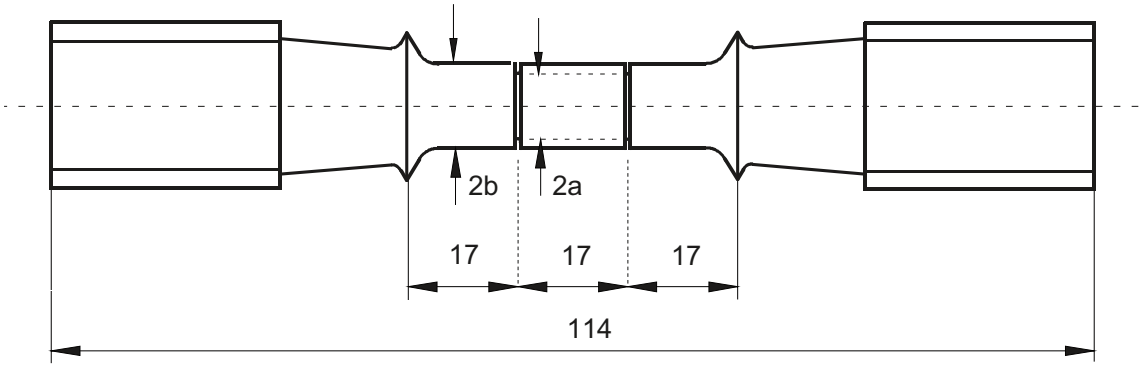

(a)

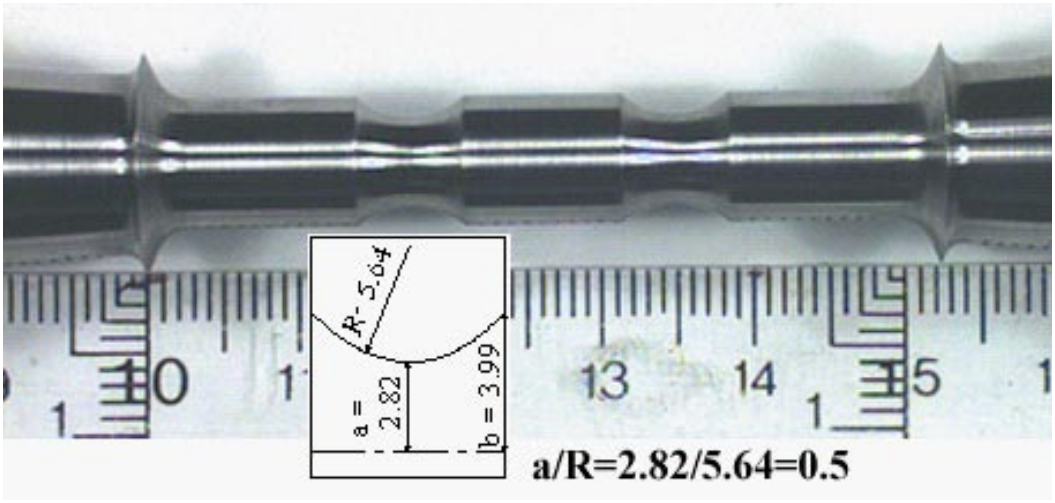

(b)

Figure 2-2. *Double notched cylindrical creep specimen. a) dimension, and b) a specimen having notch acuity a/R = 0.5 prior to test. The specimen has a diameter of 8 mm in the gauge length and a gauge length of 51 mm. The notch acuity is determined by the ratio of a/R, where the parameter a is the radius of the specimen at the base of the notch position, and R the notch root radius.*

3 Results

3.1 Creep tests

Creep testing matrix and test results under multiaxial stress state at 75°C are shown in Table 3-1. Totally, there are 20 tests. As of reporting, 8 tests are failed, 9 tests are interrupted, and 3 tests are running. All the interrupted tests are due to an unforeseen long test duration.

Creep strain as a function of time for all the tests at a given notch acuity is exhibited in Figures 3-1 to 3-4. Creep strain accounts for overall deformation within the gauge length since it is impossible to just measure the axial strain within the notch, and the axial strain within the notch is not uniform either. From Figures 3-1 to 3-4 it is seen that the primary, secondary and tertiary creep are obvious for the ruptured tests. Creep strain at rupture is larger for the blunt notch (a/R = 0.5) than that for the sharper notches.

Creep lifetime in terms of interrupted time and time to rupture is plotted as a function of net section stress in a double logarithmic scale in Figure 3-5. The creep lifetime under uniaxial stress condition is also included for comparison /7/. It can be seen that

1. the creep lifetime under multiaxial stress state for a given notch acuity increases linearly with decreasing net section stress.
2. the creep lifetime under multiaxail stress state is longer than that under uniaxial stress state, indicating notch strengthening (or in another word notch insensitivity). The notch strengthening factor in time is, for instance, greater than 70 at 180 MPa for the bluntest notch (a/R = 0.5).
3. the sharper the notch, the longer the creep lifetime is. At higher net section stresses, the sharpest notch (a/R = 18.8) has a lifetime of about 10^4 times longer than that for the bluntest notch (a/R = 0.5).

Table 3-1. Multiaxial creep testing results of copper at 75°C.

Specimen designation	*R*, mm	*a*/*R*	Net sections stress, MPa	Interrupted/rupture time, t_{MR}, h	Axial strain under loading, %	Comment
Cu-0.5-1	5.64	0.5	170	16,782	0.294	Interrupted
Cu-0.5-2			180	12,148	0.732	Interrupted
Cu-0.5-3			200	1,133	1.376	Ruptured
Cu-0.5-4			215	8	1.685	Ruptured
Cu-0.5-5			195	2,492	1.11	Ruptured
Cu-2-1	1.41	2	170	16,107	0.145	Interrupted
Cu-2-2			180	12,145	0.312	Interrupted
Cu-2-3			200	13,551	0.372	Interrupted
Cu-2-4			215	15,417	0.777	Ruptured
Cu-2-5			230	565	4.018	Ruptured
Cu-2-6			225	685	3.294	Ruptured
Cu-5-1	0.56	5	170	16,107	0.127	Interrupted
Cu-5-2			180	11,949	0.169	Interrupted
Cu-5-3			200	13,550	*	Interrupted
Cu-5-4			215	9,701	1.162	Interrupted
Cu-5-5			230	7,149 →	1.876	Running
Cu-5-6			245	20	4.032	Ruptured
Cu-18-1	0.15	18.8	230	7,146 →	1.96	Running
Cu-18-2			240	6,526 →	3.073	Running
Cu-18-3			255	147.5	6.086	Ruptured

a/R The notch acuity. The parameter *'a'* is the radius of the specimen at the base of the notch position, and *R* is the notch root radius.

* One extensometry malfunctioned under uploading.

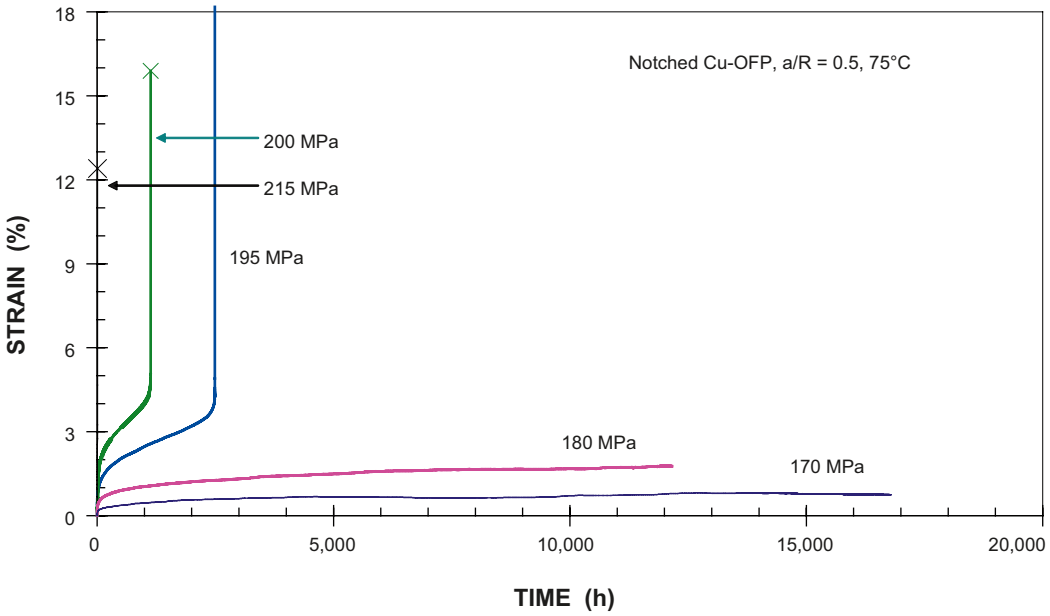

Figure 3-1. *Creep strain as a function of time for specimens having a notch acuity of 0.5 at 75°C. Two tests at 170 and 180 MPa are interrupted.*

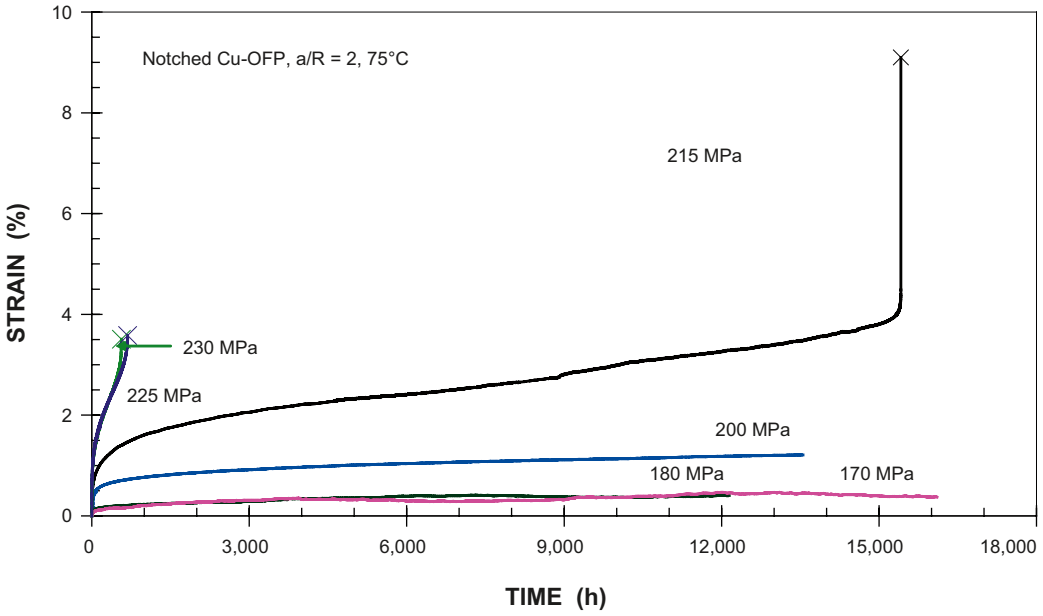

Figure 3-2. *Creep strain as a function of time for specimens having a notch acuity of 2 at 75°C. Three tests at 170, 180, and 200 MPa are interrupted.*

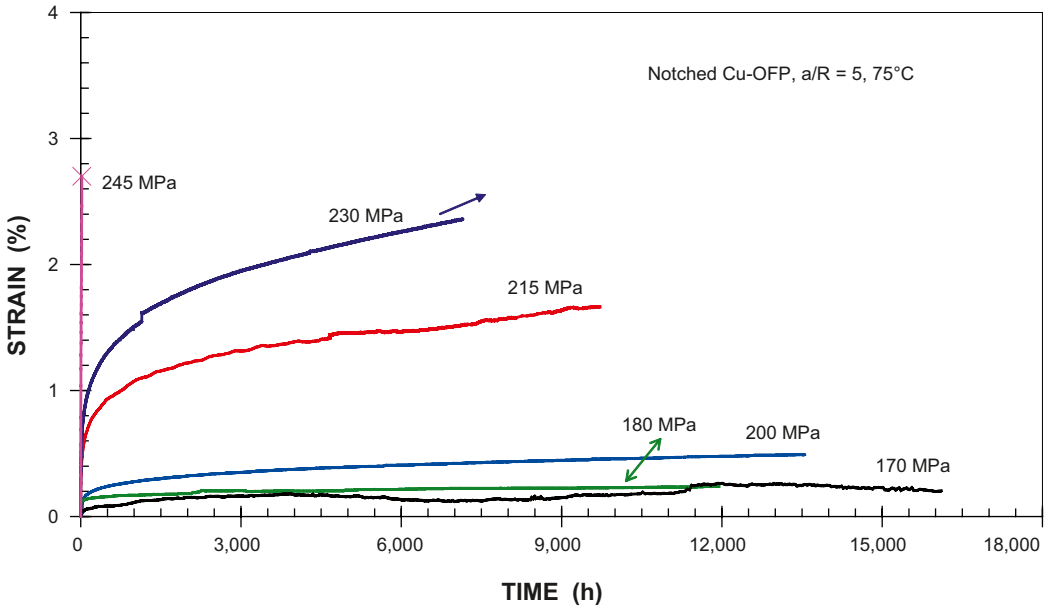

Figure 3-3. *Creep strain as a function of time for specimens having a notch acuity of 5 at 75°C. Four tests at 170, 180, 200, and 215 MPa are interrupted. The test at 230 MPa is running, indicated by an arrow.*

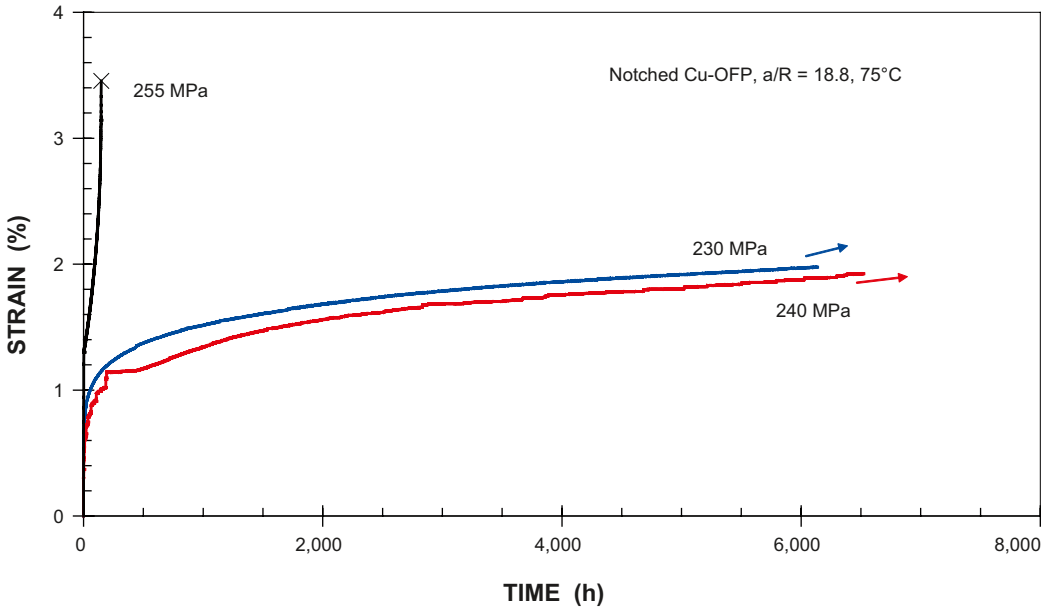

Figure 3-4. *Creep strain as a function of time for specimens having a notch acuity of 18.8 at 75°C. The tests at 230 and 240 MPa are running, indicated by arrows.*

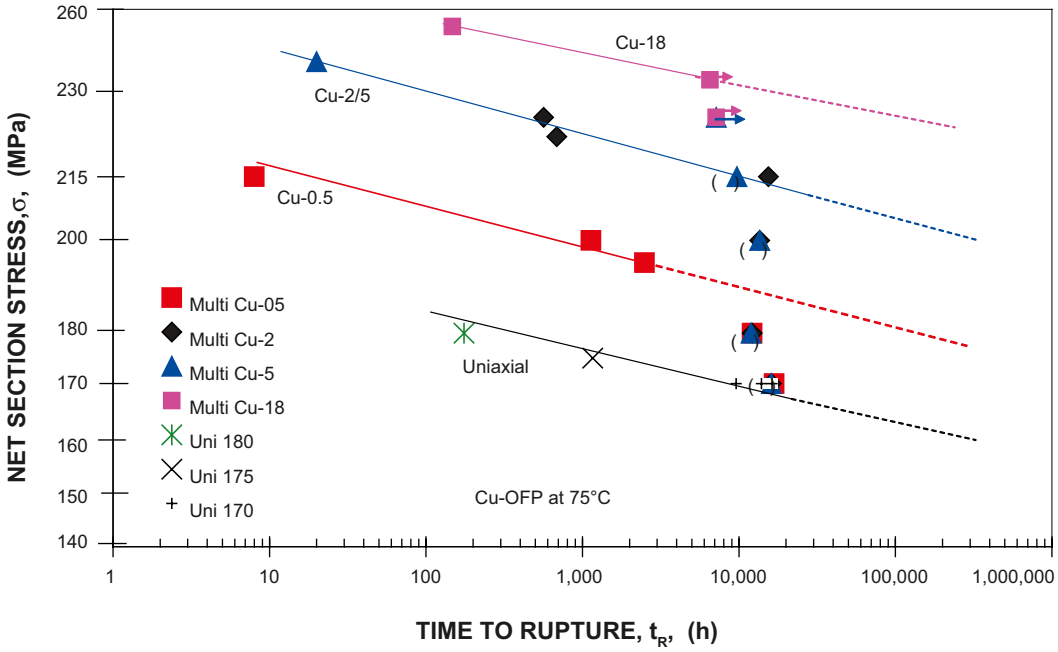

Figure 3-5. *Creep lifetime under multiaxial stress state (multi) as a function of net section stress for notched Cu-OFP at 75°C. Notch acuities are 0.5, 2, 5 and 18. Running tests are indicated by arrows, interrupted tests are in brackets. Creep lifetime under uniaxial stress state (uni) using smooth specimen is included for comparison.*

3.2 Deformation of notch

Notch dimension for all the ruptured tests before and after creep test has been measured on both notches, failed and unbroken, see Figure 3-6. The measurements are given in Table 3-2. The same measurements have also been carried out for all the interrupted tests and the results are shown in Table 3-3. Width of notch varies with varying notch acuity prior to creep test. The sharper the notch, the smaller the width is, see Table 3-2. The nominal diameter of the notches has a fixed value of 5.64 mm prior to creep test, independent of notch acuity, see Figure 2-2 and Tables 3-2 and 3-3.

It is seen from Table 3-2 that considerable creep deformation has occurred on both notches during creep test. This is even more pronounced on the failed notches. The local axial strain within the notch, ε_a, represents the notch width increase. The local radial strain within the notch, ε_r, represents the reduction of area. For the same notch acuity at the same test condition on the failed notch, ε_a and ε_r are usually more than 3 times larger than those on the unbroken one. This indicates an uneven deformation on different notches. ε_a on the failed notch increases with increasing notch acuity. For the bluntest notch ($a/R = 0.5$), ε_a is about 60%, see Table 3-2. For the sharpest notch ($a/R = 18.8$), ε_a can be as high as 780%. The ε_r on the all failed notch seems to be similar, approximately 80%, independent of notch acuity.

Unequal deformations in terms of ε_a and ε_r on two different notches are also found for interrupted tests, see Table 3-3. Although only minor differences in ε_a and ε_r are sometimes observed between the two notches after long term testing, differences in both ε_a and ε_r do exist.

Plotting ε_r against ε_a see Fig 9, it is clear that ε_r approximately increases linearly with increasing ε_a. This linear relation is notch acuity dependent and can be expressed as:

$$\varepsilon_r = a + b\varepsilon_a \qquad \text{(Eq. 3-1)}$$

In fact, a can be taken as zero. The notch acuity dependency, described by the slope b, is illustrated in Figure 3-7. ε_r increases faster than ε_a, if $b > 1$. This is the case for blunt notch, i.e. $a/R = 0.5$. Otherwise, ε_r increases slower than ε_a, if $b < 1$. This is true for sharper notches, i.e. $a/R \geq 2$.

Table 3-2. Dimension and deformation of notch before and after rupture.

Specimen	Failed notch						Unbroken notch					
	Width (mm)			Diameter (mm)			Width (mm)			Diameter (mm)		
	Before creep test	After creep test	Axial strain ε_a (%)	Before creep test	After creep test	Radial strain* ε_r (%)	Before creep test	After creep test	Axial strain ε_a (%)	Before creep test	After creep test	Radial strain ε_r (%)
Cu-0.5-4 215 MPa/ 8 hrs	7.009	8.659	23.5	5.597	1.895	88.5	6.967	**		5.614	4.623	32.2
Cu-0.5-3 200 MPa/ 1,133 hrs	6.897	11.1	60.9	5.637	**		7.349	7.88	7.2	5.621	4.907	23.8
Cu-0.5-5 190 MPa/ 2,492 hrs	7.071	**		5.624	2.181	85	7.224	8.241	14.1	5.621	4.912	23.6
Cu-2-6 225 MPa/ 685 hrs	2.832	5.998	111.8	5.652	2.315	83.2	2.813	3.773	34.1	5.704	4.946	24.8
Cu-2-4 215 MPa/ 15,417 hrs	2.790	6.070	117.6	5.631	2.359	82.4	2.816	3.369	19.6	5.654	5.042	20.5
Cu-5-6 245 MPa/ 20 hrs	1.369	4.009	192.8	5.881	2.643	79.8	1.343	1.975	47.1	5.802	5.232	18.7
Cu-18-3 255 MPa/ 148 hrs	0.324	2.851	779.9	5.748	2.699	78	0.325	1.364	319.7	5.728	4.764	30.8

* Reduction in area
** Notch has been sectioned for metallographic examination prior to measurement.

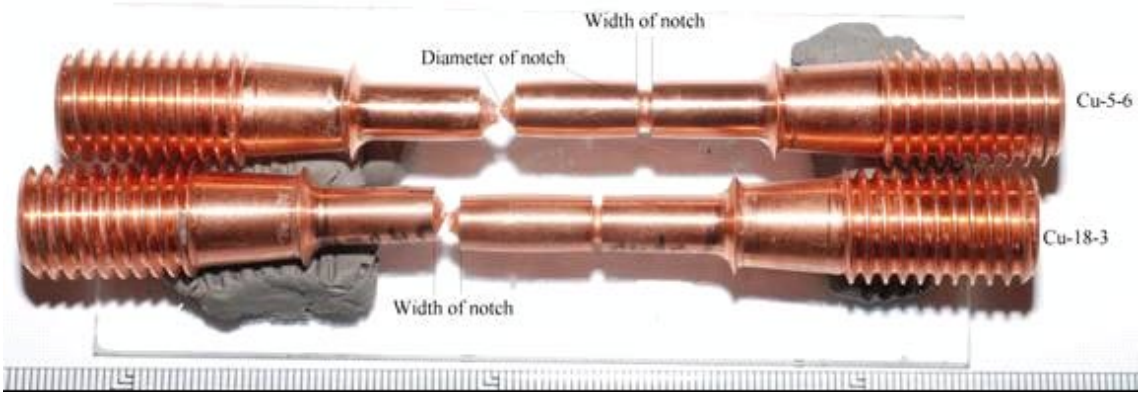

Figure 3-6. *Width and diameter of notches after creep test for two failed creep specimens.*

Table 3-3. Deformation of notch before and after interruption (unbroken specimens).

Specimen	Notch 1						Notch 2					
	Width (mm)			Diameter (mm)			Width (mm)			Diameter (mm)		
	Before creep test	After inter-ruption	Axial strain ε_a (%)	Before creep test	After inter-ruption	Radial strain ε_r (%)	Before creep test	After inter-ruption	Axial strain ε_a (%)	Before creep test	After inter-ruption	Radial strain ε_r (%)
Cu-0.5-1 170 MPa/ 16,782 h	7.017	7.132	1.64	5.612	5.395	7.58	7.161	7.239	1.09	5.593	5.374	7.68
Cu-0.5-2 180 MPa/ 12,148 h	7.142	7.656	7.20	5.623	5.074	18.57	7.284	7.872	8.07	5.607	5.070	18.24
Cu-2-1 170 MPa/ 16,107 h	2.835	2.844	0.32	5.625	5.535	3.17	2.859	2.87	0.38	5.643	5.51	4.66
Cu-2-2 180 MPa/ 12,145 h	2.765	2.847	2.97	5.662	5.426	8.16	2.798	2.951	5.47	5.667	5.513	5.36
Cu-2-3 200 MPa/ 13,551 h	2.747	2.992	8.92	5.646	5.367	9.64	2.777	3.047	9.72	5.641	5.369	9.41
Cu-5-1 170 MPa/ 16,107 h	1.148	1.161	1.13	5.643	5.558	2.99	1.135	1.148	1.15	5.661	5.572	3.12
Cu-5-2 180 MPa/ 11,949 h	1.094	1.185	8.32	5.616	5.565	1.81	1.056	1.125	6.53	5.623	5.578	1.59
Cu-5-3 200 MPa/ 13,550 h	1.042	1.159	11.23	5.666	5.513	5.33	1.042	1.206	15.74	5.635	5.474	5.63

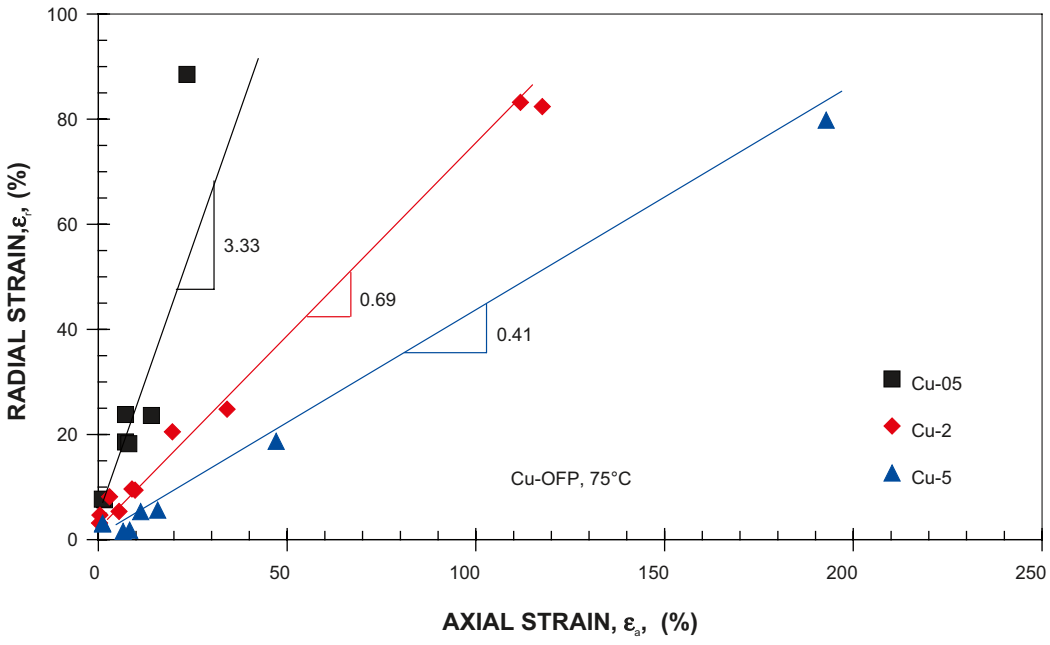

Figure 3-7. *Local axial strain within the notch, ε_a, as a function of local radial strain within the notch, ε_r. The values of ε_a and ε_r are taken from both interrupted and ruptured tests at 75°C. Both notches are taken into account.*

3.3 Post test metallography

All the failed specimens are metallographically examined. Transgranular failure is predominant, insensitive to stress, rupture time, as well as notch acuity, see Figures 3-8a, 3-8b, 3-9a, 3-9d, 3-10a, 3-11a, and 3-12a. Adjacent to fracture, elongated grains along the stress direction and separate pores and cavities to a small extent are observed, see Figures 3-8b, 3-8c, 3-9a, 3-9d, 3-10a, 3-11a, and 3-12a. On the unbroken notch, there is no creep damage visible for the bluntest notch ($a/R = 0.5$), see Figure 3-8d. For the sharper notch ($a/R > 2$), separate cavities to a small extent are observed on the grain boundary on the unbroken notch, see Figures 3-9b, 3-9c, 3-10b, 3-11b, and 3-12b. The cavities are usually found approximately 0.5–1 mm below the outer surface, *c. f.* Figure 3-9b. For the long term testing, intergranular crack is found on the unbroken notch, see Figure 3-9 (e).

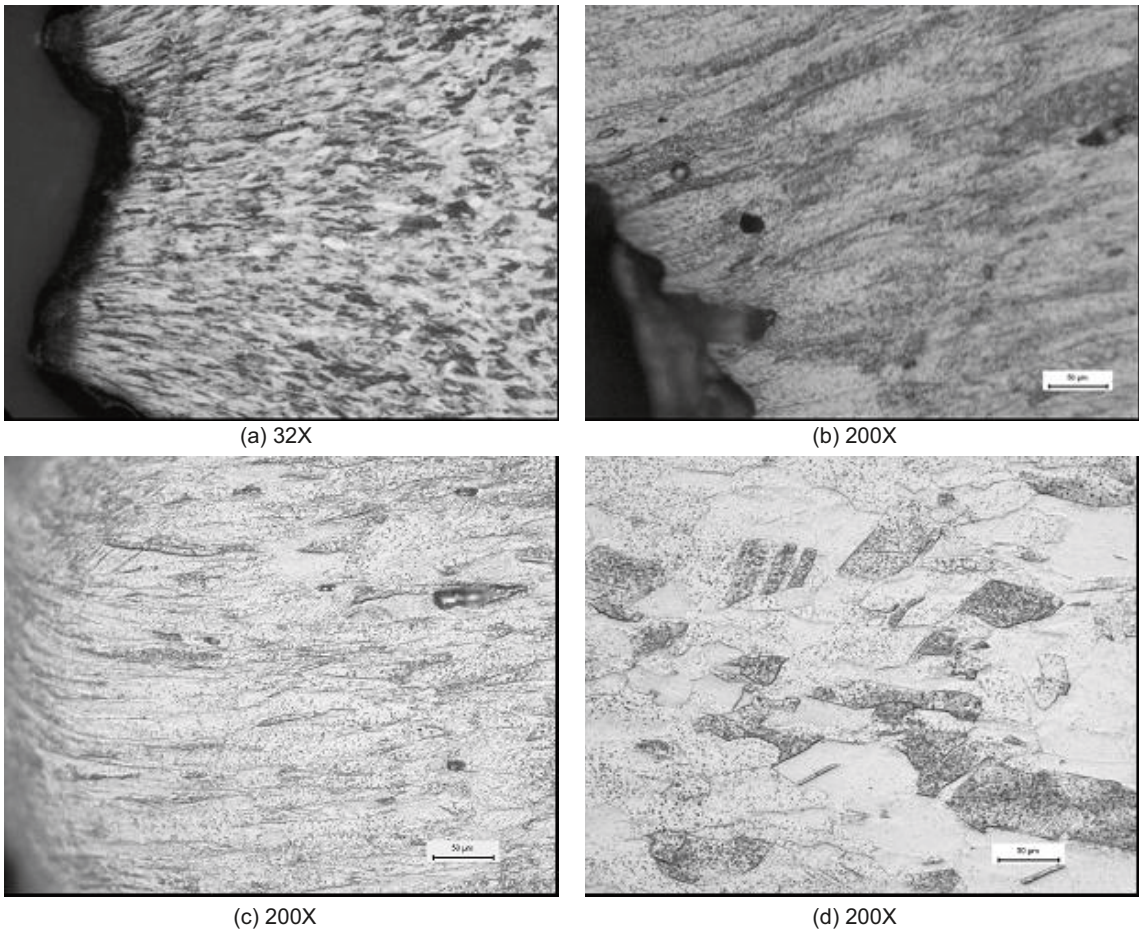

(a) 32X (b) 200X

(c) 200X (d) 200X

Figure 3-8. *LOM images showing (a) Specimen Cu-05-5, 195 MPa, failed after 2,492 hrs, elongated grains adjacent to fracture. (b) Same as (a), few pores and cavities. (c) Specimen Cu-05-3, 200 MPa, failed after 1,133 hrs, elongated grains and few pores and cavities adjacent to fracture. (d) Same as (c). Unbroken notch. Deformed grains and damage-free.*

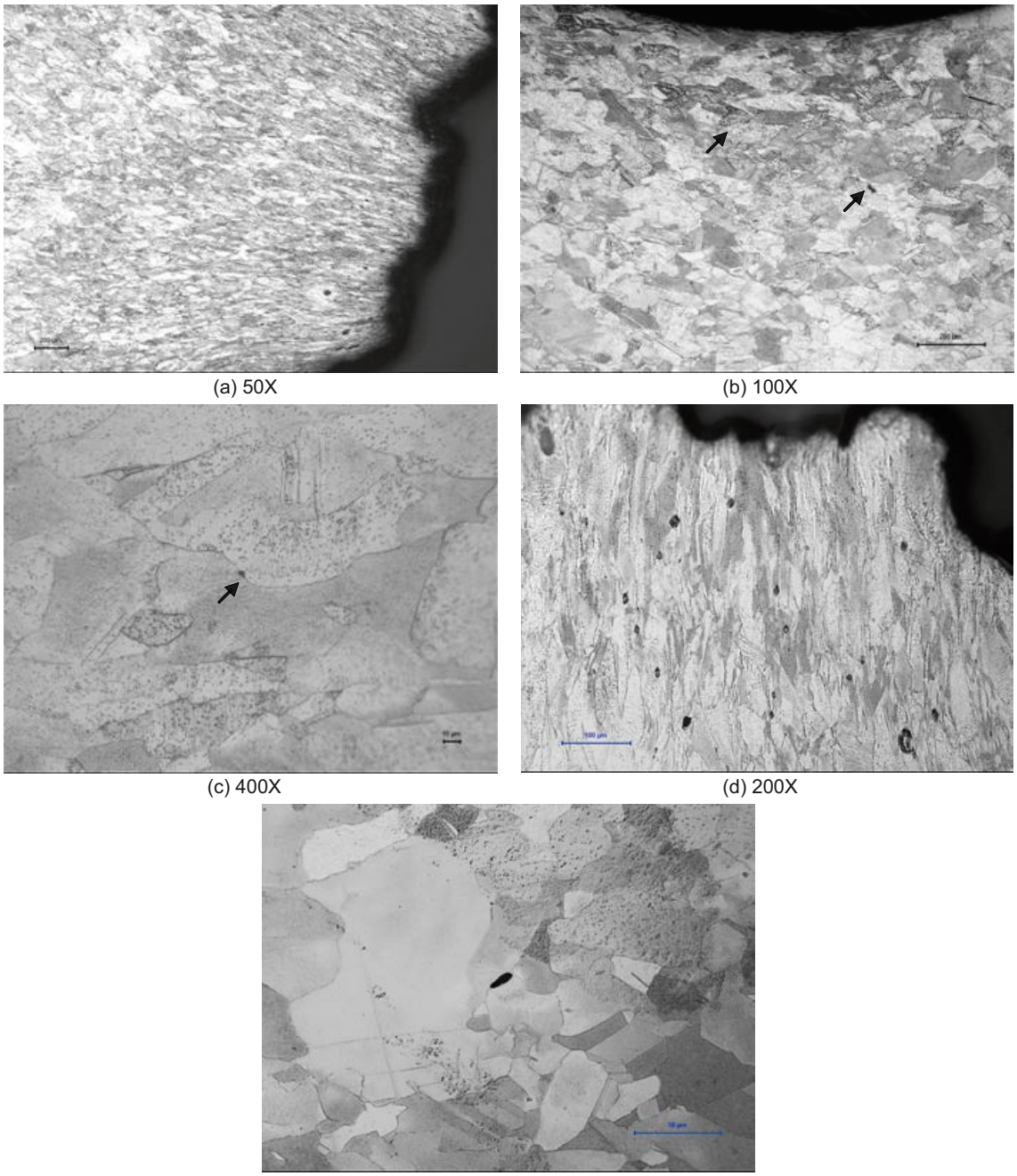

Figure 3-9. *(a)–(c) specimen Cu-2-5, 235 MPa, failed after 565 hrs. LOM images showing (a) elongated grains and few pores and cavities near fracture. (b) Unbroken notch. Few separate cavities at grain boundary, indicated by arrows. (c) Same as (b), but higher magnification. (d)–(e) specimen Cu-2-4, 215 MPa, failed after15,417 hrs. LOM images showing (d) elongated grains and few pores and cavities near fracture. (e) Unbroken notch. Intergranular crack.*

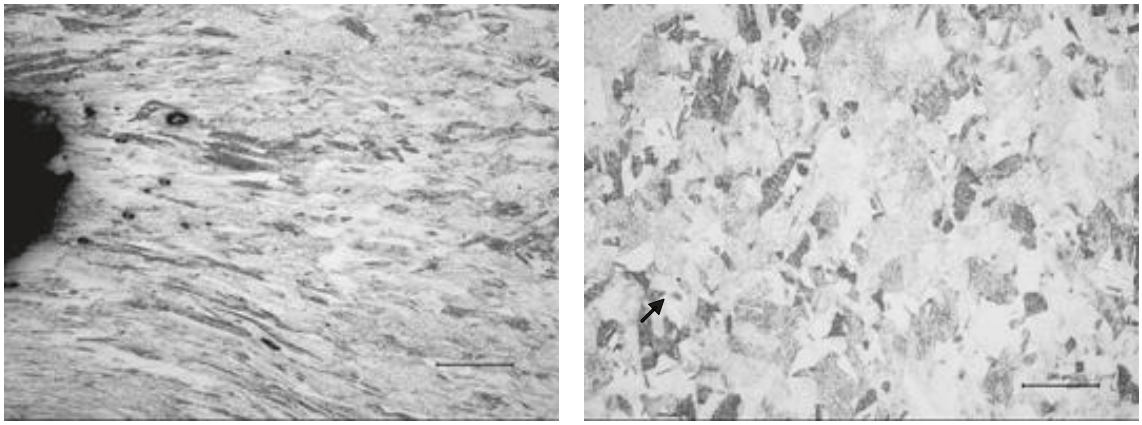

(a) 100X (b) 100X

Figure 3-10. *Specimen Cu-2-6, 225 MPa, failed after 685 hrs. LOM images showing (a) elongated grains and few pores and cavities near fracture. (b) Unbroken notch. Few separate cavities at grain boundaries, indicated by arrow.*

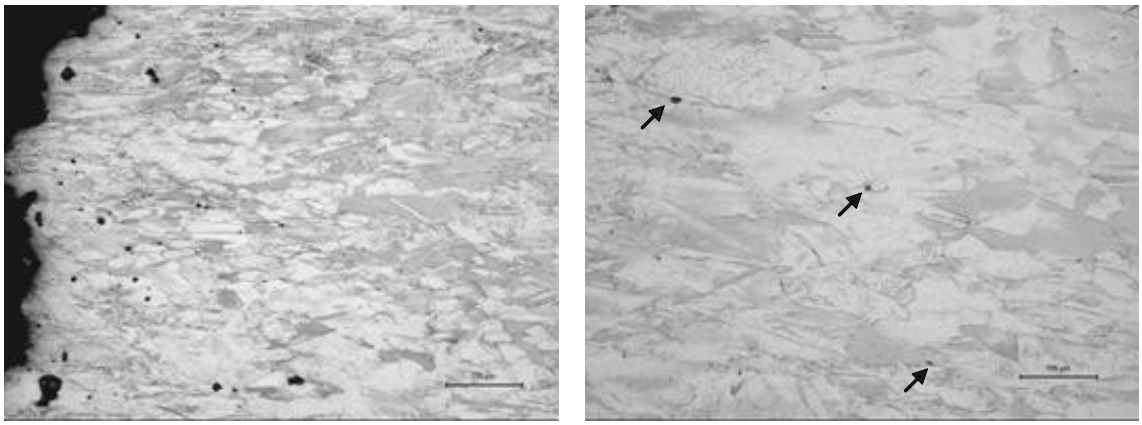

(a) 100X (b) 200X

Figure 3-11. *Specimen Cu-5-6, 245 MPa, failed after 20 hrs. LOM images showing. (a) elongated grains and few pores and cavities near fracture. (b) Unbroken notch. Few separate cavities at grain boundaries, indicated by arrow.*

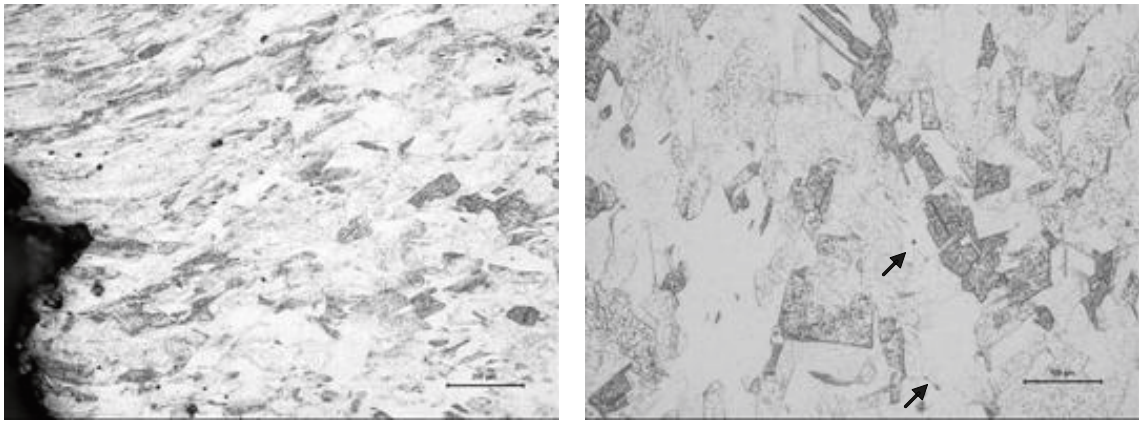

(a) 100X (b) 200X

Figure 3-12. *Specimen Cu-18-3, 255 MPa, failed after 148 hrs. LOM images showing. (a) elongated grains and few pores and cavities near fracture. (b) Unbroken notch. Few separate cavities at grain boundaries, indicated by arrow.*

4 FEM Simulations

4.1 Constitutive equation

The notched bar creep tests have been analysed with the help of FEM simulations. The principles followed in the analysis are described in /9/–/11/. A FEM program that allows large deformations has been used. A fundamental equation for stationary creep in pure copper is the basis for the constitutive equation /12/

$$\dot{\varepsilon}_{OFP} = \frac{2bc_L}{m}\frac{D_{s0}b\tau_L}{k_BT}\left(\frac{\sigma}{\alpha Gb}\right)^3 e^{\frac{\sigma b^3}{k_BT}} e^{-\frac{Q}{RT}\left[1-\left(\frac{\sigma}{\sigma_{i\max}}\right)^2\right]} / f_P = h(\sigma) \qquad \text{(Eq. 4-1)}$$

The interpretation of the parameters in Equation 4-1 can be found in Table 4-1. $\dot{\varepsilon}_{OFP}$ is the creep strain rate of Cu-OFP, σ the applied stress and T the temperature. An abbreviation $h(\sigma)$ is introduced for the expression in Equation 4-1.

In our previous FEM analysis of the copper canister, a primary creep model based on the Φ model has been used /12/, /13/. In the present analysis a recently developed fundamental model is applied instead. A fundamental model for tensile and compressive flow stress curves is the starting point /14/.

$$\sigma = \sigma_y + (\sigma_{creep} - \sigma_y)(1 - e^{-\omega\varepsilon}) \qquad \text{(Eq. 4-2)}$$

where σ_y is the yield strength, σ_{creep} the stress giving the same creep rate as in the tensile test and ω a constant. For a given strain rate and temperature, σ_{creep} is found by iteration from Equation 4-1. Also the yield strength is temperature and strain rate dependent. An expression for this dependence can be found in /14/. ω is given by /14/

$$\omega = \frac{m}{b} d_{int}\left(2 - \frac{1}{n_{slip}}\right) \qquad \text{(Eq. 4-3)}$$

m is the Taylor factor (= 3.06), d_{int} the interaction distance between dislocations (=2.5 b) and n_{slip} the number of independent slip systems (= 12 for fcc-metals). The resulting value is ω = 14.66. From Equation 4-3 the creep stress σ_{creep} can be determined. It is inserted into Equation 4-1

$$\frac{d\varepsilon_c}{dt} = h\left(\sigma_y e^{-\varepsilon} + \frac{\sigma - \sigma_y e^{-\varepsilon}}{1 - e^{-\omega\varepsilon}}\right) \qquad \text{(Eq. 4-4)}$$

Table 4-1. Interpretation of parameters and values used in Equation 4-1.

Parameter description	Parameter	Value
Burgers vector	b	$2.56\cdot10^{-10}$ m
Taylor factor	m	3.06
Boltzmann's constant	kB	$1.381\cdot10^{-23}$ J/grad
Shear modulus	G	$G = 4.75\cdot10^4 - 17T$ MPa, T in K
Dislocation line tension	τL	$7.94\cdot10^{-16}$ MN at RT
Coefficient for self diffusion	D_{s0}	$1.31\cdot10^{-5}$ m²/s
Activation energy for self diffusion	Q	198,000 J/mol
Strain hardening constant	cL	57
Constant	α	0.19
Max back stress	σ_{imax}	257 MPa
Influence of phosphorus	fP	3,000 for T < 125ºC

The factor $e^{-\varepsilon}$ takes into account the fact that engineering stresses are assumed to be used in Equation 4-4 instead of the true stresses in Equation 4-2. Equation 4-4 is a differential equation for the creep strain as a function of time. It has been used to successfully to represent uniaxial creep curves for Cu-OFP in the temperature interval 75 to 250°C /15/.

The models Equation 4-1, Equation 4-2, and Equation 4-4 are referred to as fundamental. The reason is that they are based on fundamental physical principles and that no fitting parameters are involved.

With the help of Odqvist's equation, Equation 4-4 can be transformed to multiaxial stress states

$$\frac{d\boldsymbol{\varepsilon}_c}{dt} = \frac{3}{2}\frac{d\varepsilon_c^{eff}}{dt}\frac{\boldsymbol{\sigma}'}{\sigma_{eff}} \qquad \text{(Eq 4-5)}$$

where $\boldsymbol{\varepsilon}_c$ is the creep strain tensor, σ_{eff} the effective (von Mises) stress and $\boldsymbol{\sigma}'$ the stress deviator tensor. The effective creep strain rate is given by

$$\frac{d\varepsilon_c^{eff}}{dt} = h(\sigma_y e^{-\varepsilon} + \frac{\sigma_{eff} - \sigma_y e^{-\varepsilon}}{1 - e^{-\omega\varepsilon}}) \qquad \text{(Eq 4-6)}$$

Equation 4-5 was used in the FEM creep analysis below. To determine the direct effect when the specimens are loaded, elasto-plastic analysis was applied. Equation 4-2 was used to describe the stress strain curve.

4.2 Creep curves

In the FEM analysis of the notched bars, the cylinder symmetry is taken into account. The geometry of the specimens is given in Figure 2-2 and Table 3-1. It has also been assumed that the specimens are symmetric on both sides of the notches. This is only approximately correct. The specimens contain two notches and there is no perfect symmetry around each notch. Since a large number of creep calculations have been performed for each of the 20 specimens, this approximation has been chosen. The number of degrees of freedom in the computations has been about 30,000.

On loading there is a pronounced stress concentration at the notch. This is exemplified in Figures 4-1a and 4-2a. The stress distributions in Figures 4-1a and 4-2a have been determined with elasto-plastic analysis.

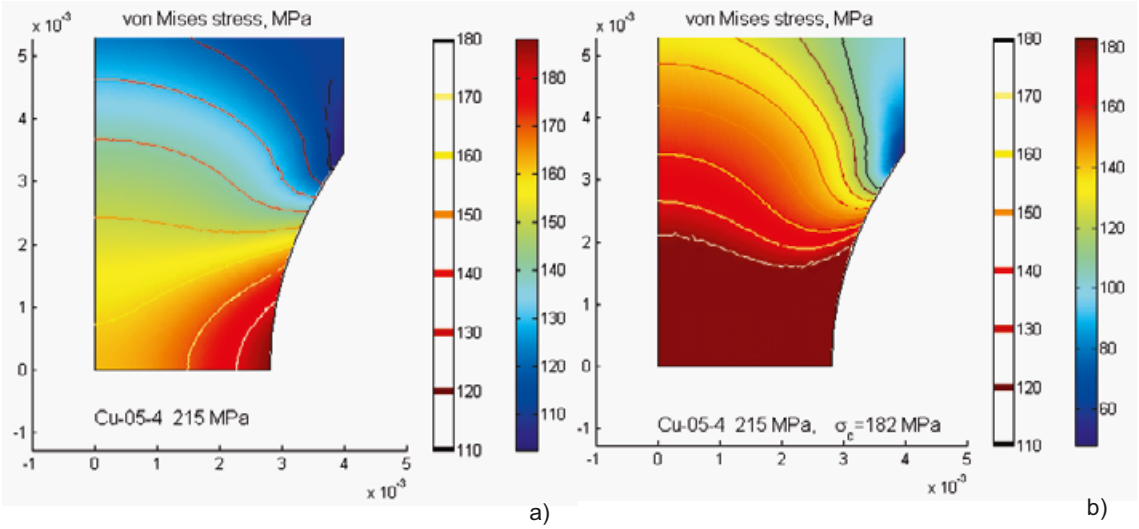

Figure 4-1. *von Mises stress distribution for specimen Cu-05-4 with an acuity of 0.5 and a net section stress of 215 MPa. The radial and axial coordinates r and z are on the axes with origin at the centre of the notch. a) Directly after loading, b) after a stationary creep stress σ_c=182 MPa has been reached.*

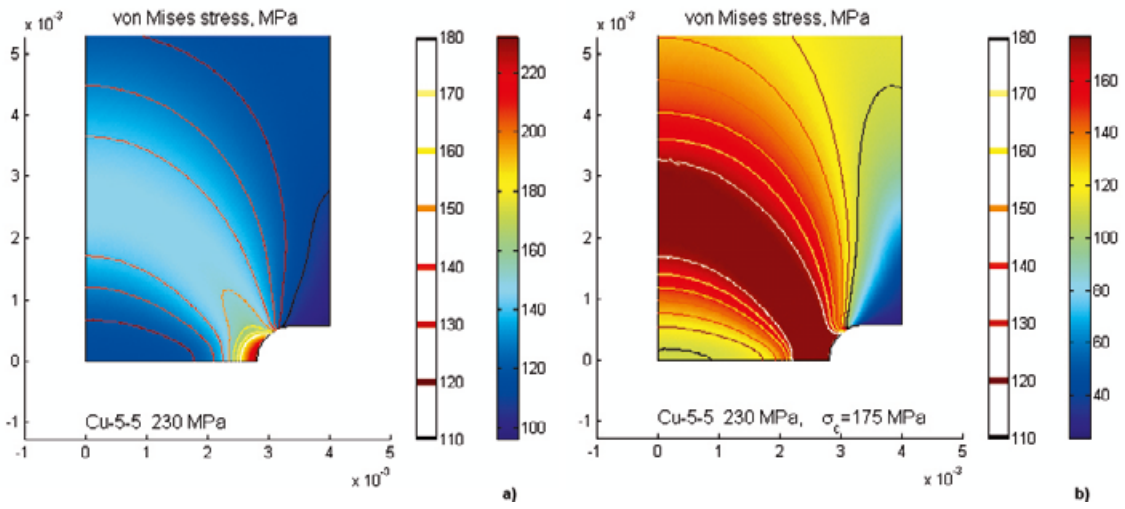

Figure 4-2. *von Mises stress distribution for specimen Cu-5-5 with a notch acuity of 5 and a net section stress of 230 MPa. The radial and axial coordinates r and z are on the axes with origin at the centre of the notch. a) Directly after loading, b) after a stationary creep stress* σ_c*=175 MPa has been reached.*

This type of stress distribution gives rise to inhomogeneous creep. Outside the notch there will hardly be any creep deformation. In the notches the creep rate would be very high if these local areas could be deformed independently. Since this is not possible, stress relaxation will take place and the remainder of the section will take a higher load. Eventually stress redistribution occurs and in a band across the specimen, the effective stress becomes almost constant. This is illustrated in Figures 4-1b and 4-2b. This process is typically fast and appears after about $t_R/100$, where t_R is the rupture time.

For specimens with the acuity 0.5, the band with the constant stress lies across the centre of the notch, see Figure 4-1b. On the other hand for the specimens with acuities of 2, 5 and 18, the band takes almost a spherical form, see Figure 4-2b. In both situations the band is fairly wide. When this stationary situation is reached, the specimens are free to creep in the axial direction. It should be noticed that the width of the band in the axial direction is fairly constant, which helps the creep deformation.

The model results are compared to the experimental data for specimens with notch acuity of 0.5 in Figure 4-3. Except for the test with the lowest net section stress, the model seems to underestimate the creep rate. In the model only primary and secondary creep is taken into account, so the tertiary creep observed in three of the tests with the highest net section stress is not covered.

As is evident from Figure 4-1b, the creep deformation is much higher in the centre of the notch than elsewhere. The specimen appears to be softer at the notch, which gives rise to early necking. This is not taken into account in the model, and can be the reason why the model underestimates the creep rate at higher stresses.

The model overestimates the strain on loading at the lowest net section stress but gives reasonable values at the higher stresses.

In Figure 4-4 creep curves for specimens with notch acuity of 2 are analysed. The model gives a fairly accurate representation of the creep rate, i.e. the slope of the curves. The strain on loading is however overestimated at low net section stresses and underestimated at higher net section stresses. This reason for the deficiency is not known. The predicted strain on loading agrees with that obtained from elasto-plastic analysis.

The model values for the creep strain are compared to the experimental data for specimens with notch acuity of 5 in Figure 4-5. In the same way as for an acuity of 2, the creep rate is predicted in an acceptable manner. The loading strain is however underestimated for the lower net section stresses.

In the specimens with an acuity of 18.8, the notch is quite sharp. Its radius is only 0.15 mm. In spite of this, the creep model can reproduce the experimental creep strain data quite well, Figure 4-6. The creep rates are in good agreement and the loading strains only differ significantly at the highest net section stress.

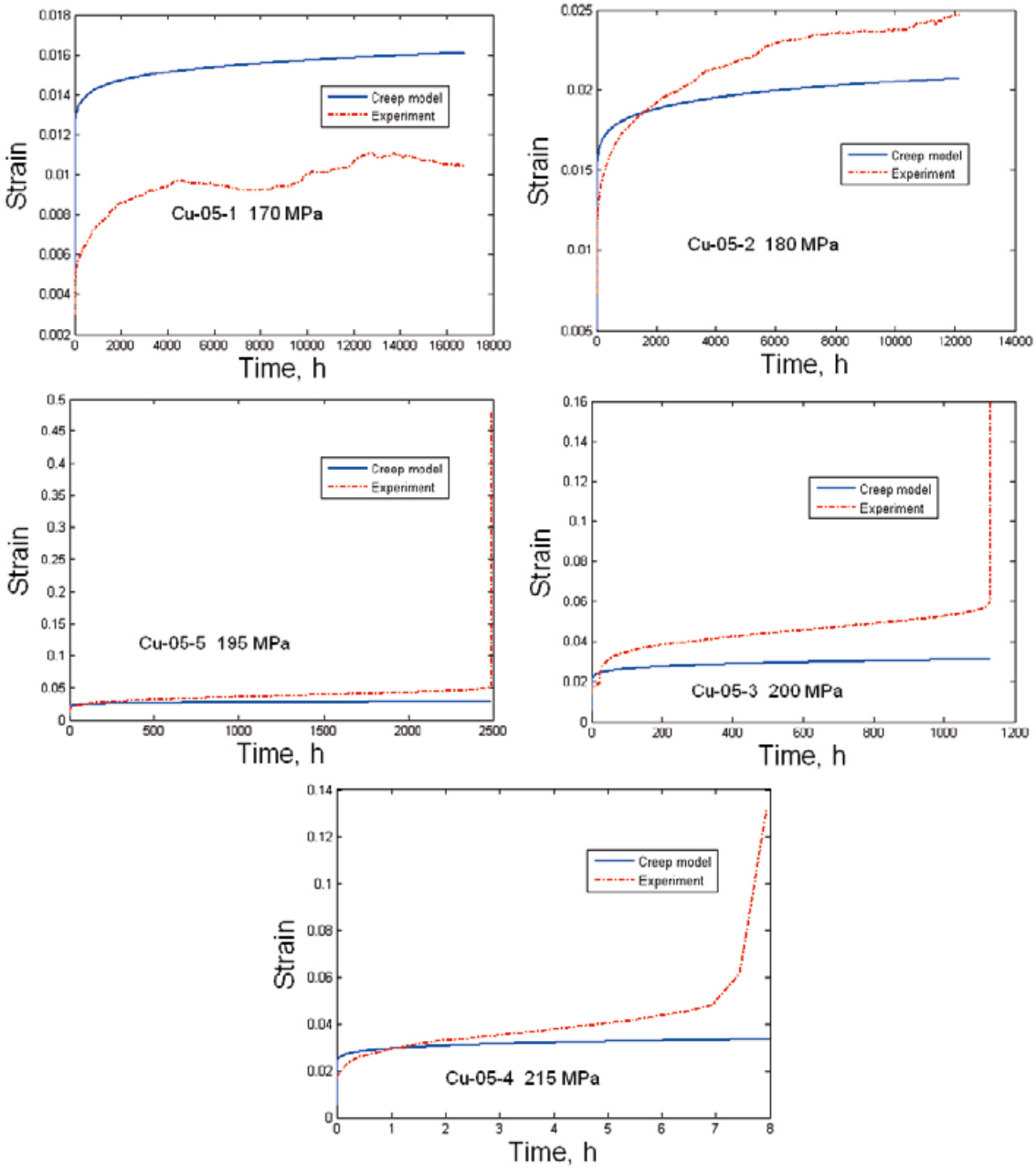

Figure 4-3. *Creep strain versus time for the five specimens with a notch acuity of 0.5. The model in Equation 4-5 is compared to experimental data. The specimen designation and net section stress are given in the figures.*

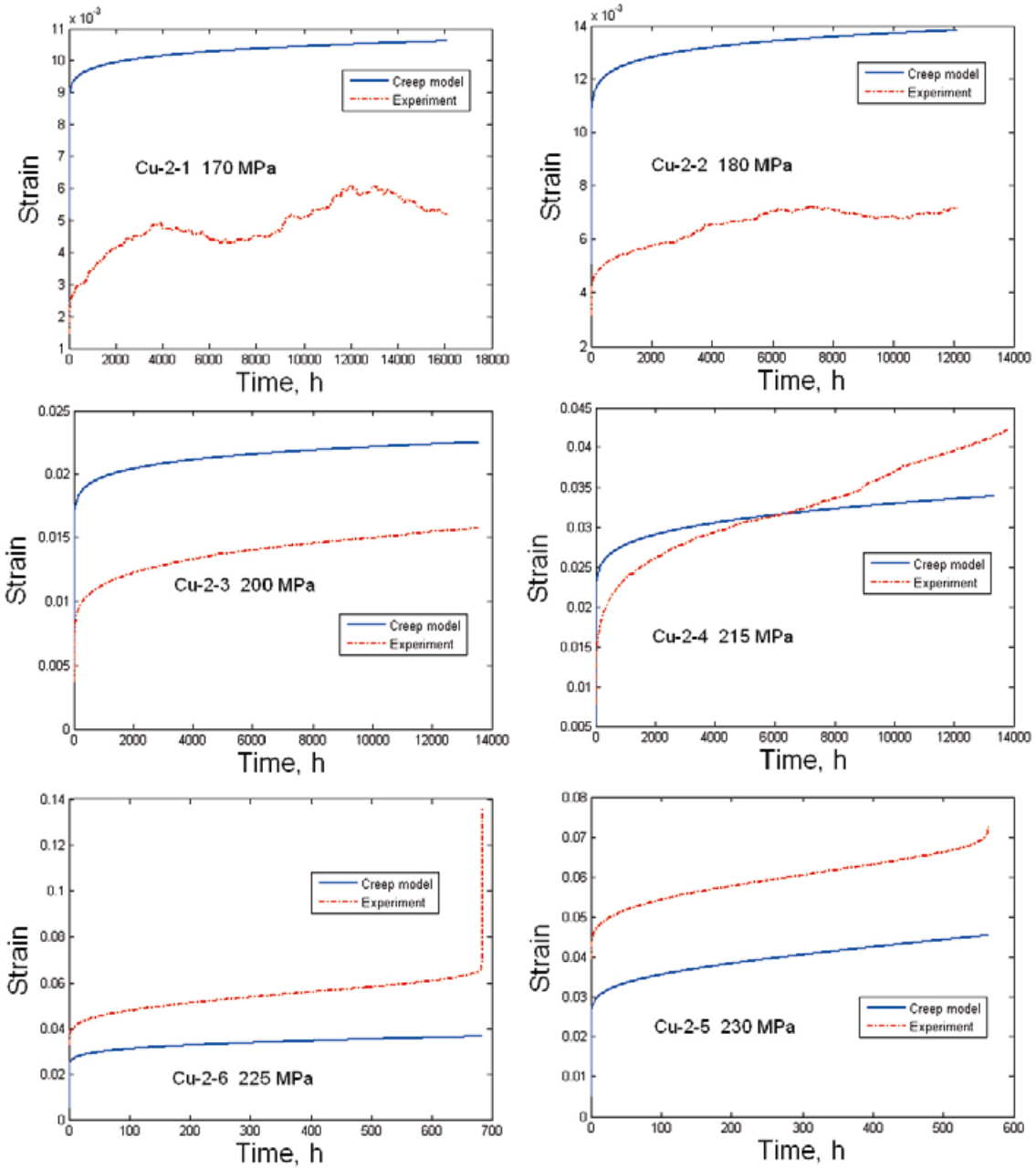

Figure 4-4. *Creep strain versus time for the six specimens with a notch acuity of 2. The model in Equation 4-5 is compared to experimental data. The specimen designation and net section stress are given in the figures.*

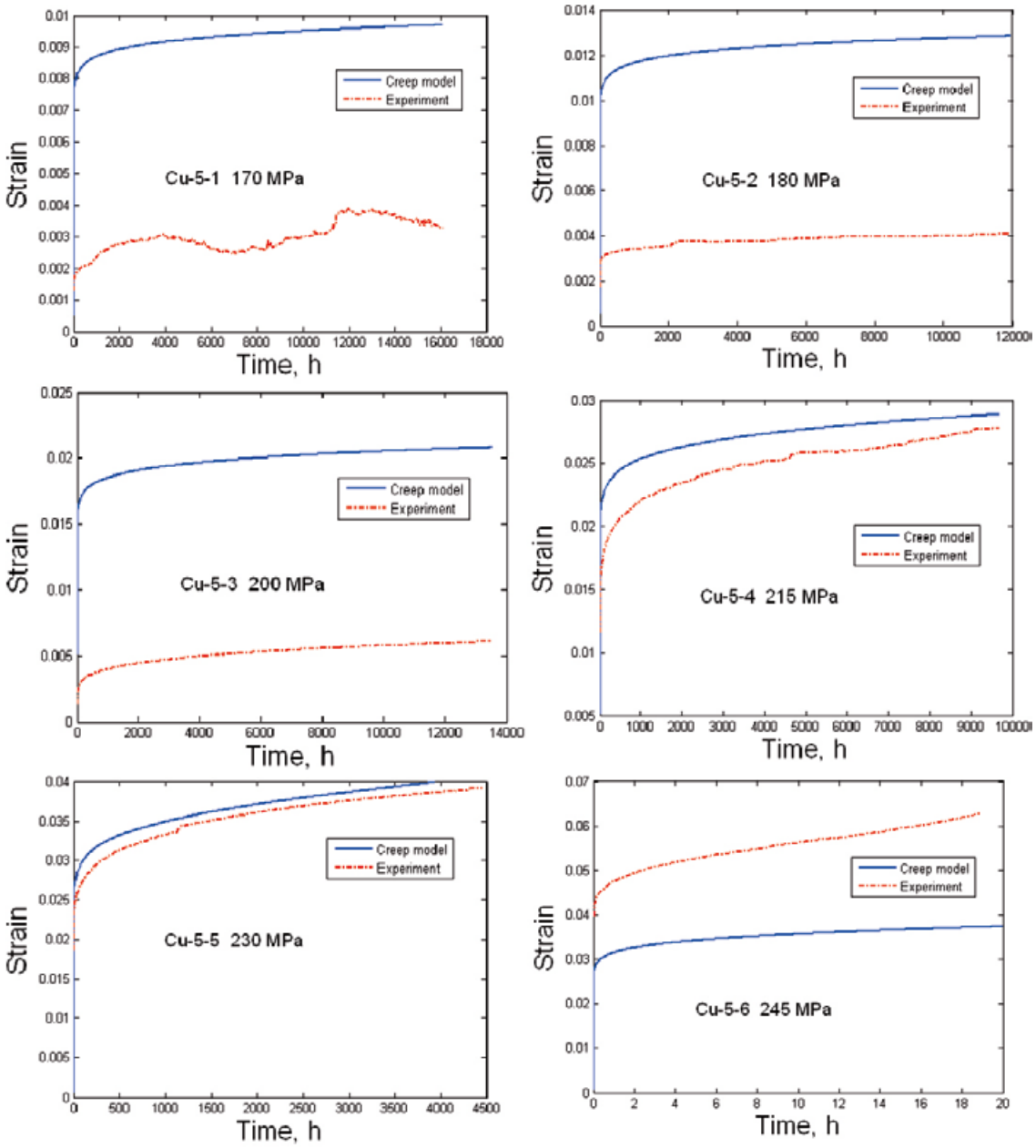

Figure 4-5. *Creep strain versus time for the six specimens with a notch acuity of 5. The model in Equation 4-5 is compared to experimental data. The specimen designation and net section stress are given in the figures.*

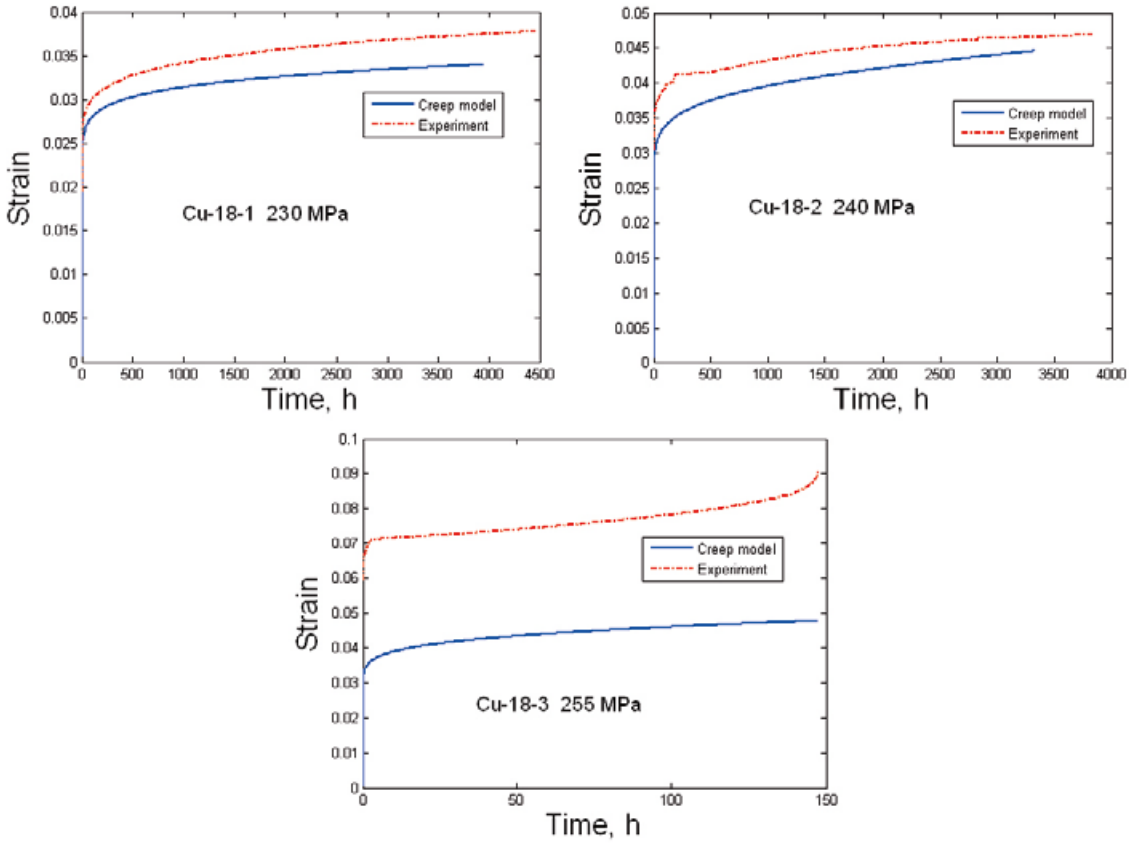

Figure 4-6. *Creep strain versus time for the three specimens with a notch acuity of 18.8. The model in Equation 4-5 is compared to experimental data. The specimen designation and net section stress are given in the figures.*

4.3 Creep rupture

In the previous section it was demonstrated that the creep model Equation 4-5 could represent the creep strain versus time curves in a satisfactory manner. Since tertiary creep is not included in the model, it cannot be used to predict rupture. Instead the stationary creep stresses σ_c will be used. σ_c is the stationary effective stress that is reached after the initial redistribution of stresses, see Figures 4-1b and 4-2b. The creep exponent of Cu-OFP is about 65 at 75°C. This high creep exponent implies that the creep rate is approximately constant for a constant σ_c.

σ_c is compared with uniaxial creep rupture data in Figure 4-7. The σ_c values are listed in Table 4-2. The uniaxial data are for forged and extruded Cu-OFP at 75°C /7/. The values for notched bars are grouped in two categories. For specimens with notch acuity of 0.5, a homogeneous stress distribution is obtained at the centre of the notch. This is referred to as waist deformation, see Figure 4-1b. For the higher acuities 2, 5, and 18.8 the constant stress appears in a spherical band, see Figure 4-2b. This is referred as to band deformation.

In the case of band deformation, the stationary stresses σ_c fall approximately on the band for the uniaxial data in Figure 4-7. In this case if σ_c is inserted in the uniaxial creep rupture curve, an approximate time to rupture is obtained. Since σ_c lies slightly above the uniaxial curve, this approach should be conservative.

In the case of waist deformation, σ_c lies 3 to 5% below the uniaxial curve. With the type of stress distribution in Figure 4-1b, the creep deformation is strongly concentrated to the centre of the notch. This will give rise necking and early plastic collapse of the specimen. This is believed to be the reason for the lower rupture stresses.

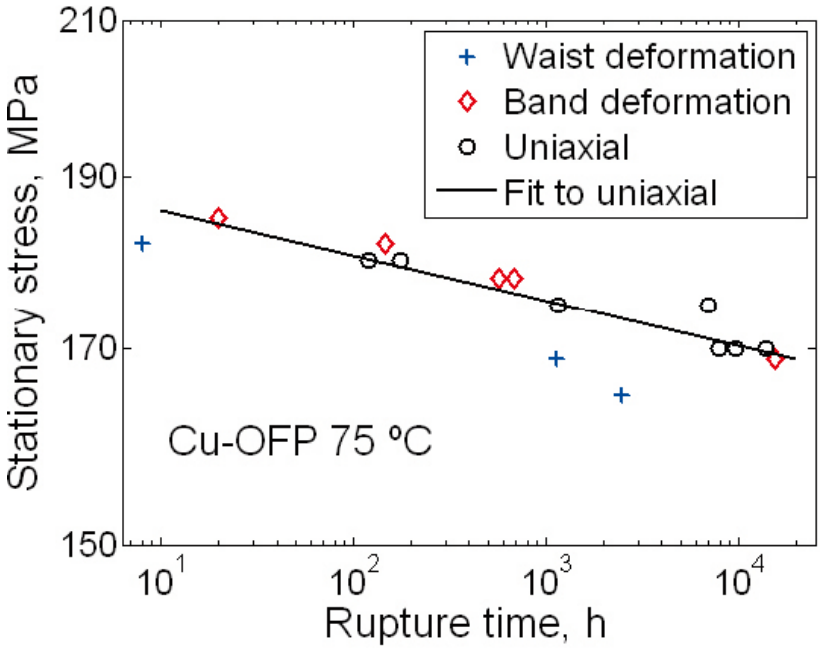

Figure 4-7. *Creep stress versus rupture time. The experiments are uniaxial data for Cu-OFP at 75°C /7/. For notched bar specimens the stationary stress σ_c is given as function of rupture time. Waist deformation represents notch acuity of 0.5, and band deformation notch acuities of 2, 5, and 18.8.*

If the creep exponent $n = \infty$, the steady state stress field giving stationary creep deformation has the same form as the stress field at plastic collapse for a rigid plastic solid, but with the yield strength σ_y replaced by the reference stress σ_{ref}.

$$\sigma_{ref} = \frac{P\sigma_y}{P_L} \qquad \text{(Eq. 4-7)}$$

P is the applied load and P_L is the limit load for a rigid plastic material yielding at the yield strength. Reference stress values for the notched specimens are given in Table 4-2. Since the creep exponent is very high $n = 65$ in the present study, the stationary creep σ_c is quite close to the reference stress

$$\sigma_c \approx \sigma_{ref} \qquad \text{(Eq. 4-8)}$$

For uniaxial specimens the reference stress is equal to the applied axial stress. In Figure 4-8 the relation between the reference stresses and the observed rupture times is shown. It is obvious that the reference stress can be used to estimate the rupture times.

Running and interrupted specimens are included in Figure 4-8. The relation between the reference stress and the rupture time was unknown before the start of the project. In retrospect it can be concluded that the applied load on the interrupted specimens was too low to reach rupture in reasonable time.

Reference stress is quite a useful concept for many components with simple geometry. However, it is difficult to apply to components with more complex geometry. First the net section stress can be considered instead. If it does not exceed the uniaxial rupture stress, failure is very unlikely, see Figure 3-5. Second, in the case when stationary creep stresses are established, the failure will take place where the stationary stresses are highest and significant tensile stresses are present. Using these stresses the rupture time can be estimated with the help of a rupture plot of the type in Figure 4-7. If stationary stresses are not established, the creep damage has to be integrated as a function of time at critical positions using the effective stress.

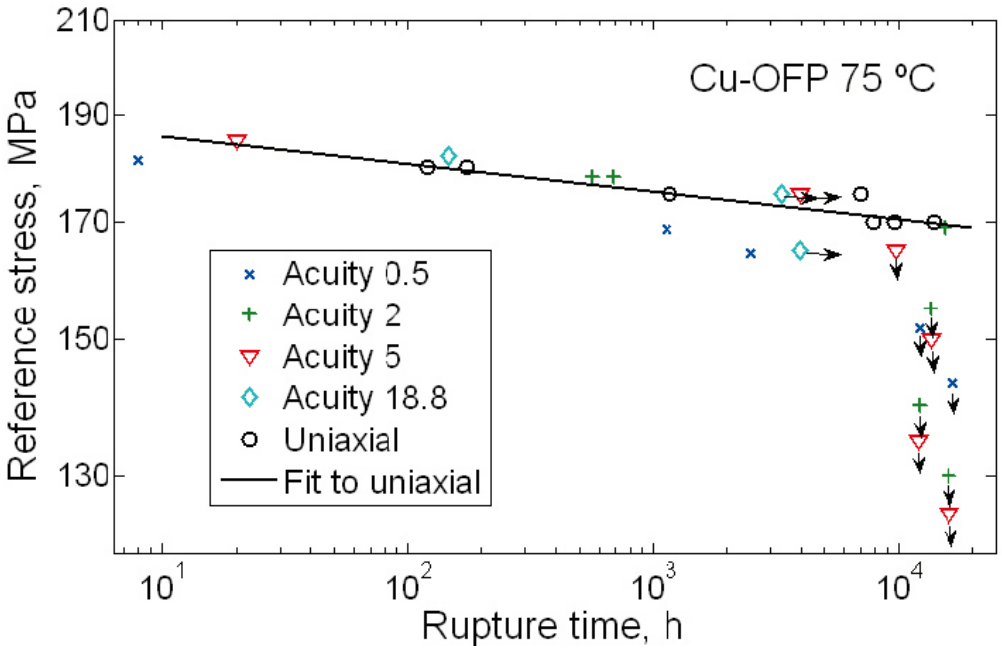

Figure 4-8. *Reference stress σ_{ref} versus rupture time for specimens with notch acuities 0.5, 2, 5, and 18.8. For comparison uniaxial data for Cu-OFP at 75ºC are included /7/. Running and interrupted specimens are marked with a horizontal and vertical arrow, respectively.*

4.4 Shape changes

Observed shape changes in the notched bar specimens during creep testing can be found in Table 3-3. They are also summarised in Table 4-2 together with the model results. Values are given for the displacement and reduction of area across the notches. As expected both the displacement and the reduction in area increase with increasing net section stress. The experimental values for the ruptured notches are in general larger than for the corresponding unbroken notch on the same specimen. This is a pronounced effect at larger stresses, which is likely to be due to necking. Since necking is not taken into account explicitly in the computation, the model values should primarily be compared with the data for the unbroken notches.

Two types of model values are given: i) those computed with the creep model Equation 4-5 representing the total creep deformation at rupture or when the test was interrupted; ii) the deformation on loading that is computed with elasto-plastic analysis. Since the creep model includes the loading strain, the creep result represents the total deformation, and that is the value that should be compared to the experimental values (for the unbroken notch).

Concerning the displacement across the notches (increase in width) the model values give a reasonable estimate of the observed deformation. The main exception is the specimens with the lowest net section stress. The experimental values are then considerably smaller. They are even smaller than the values from the elasto-plastic analysis. The loading strain gives always a significant contribution to the total creep strain.

The observed values for the reduction in area are in most cases well reproduced by the model. The deviations are primarily for the largest experimental values. The influence of necking is the probable cause of these deviations. Contrary to the case with the displacements, the loading strain only plays a minor role.

Table 4-2. Observed and modelled shape changes.

Experiment				Model		Displacement across notch, mm				Reduction in area, %			
						Experiment		Model		Experiment		Model	
Specimen	Net section stress, MPa	Rupture time, h	k_R	Reference stress σ_{ref}, MPa	Stationary creep stress σ_c, MPa	Ruptured notch	Unbroken notch	Creep	On loading	Ruptured notch	Unbroken notch	Creep	On loading
Cu-05-1	170	16,782	–1	143.4	143	0.115	0.078	0.42	0.21	7.58	7.68	10.5	3.0
Cu-05-2	180	12,148	–1	151.8	151	0.514	0.588	0.6	0.24	18.57	18.24	13.5	3.4
Cu-05-5	195	2,492	1	164.5	165	-	1.017	0.76	0.29	85	23.6	19	4.1
Cu-05-3	200	1,133	1	168.7	169	4.203	0.531	0.84	0.31	-	23.8	21	4.3
Cu-05-4	215	8	1	181.4	182	1.65	0	0.85	0.37	88.5	32.2	22	5.0
Cu-2-1	170	16,107	–1	132.3	130	0.009	0.011	0.13	0.10	3.17	4.66	4.3	0.8
Cu-2-2	180	12,145	–1	140.1	140	0.082	0.153	0.17	0.12	8.16	5.36	5.3	1.0
Cu-2-3	200	13,551	–1	155.6	155	0.245	0.27	0.36	0.21	9.64	9.41	8.5	1.9
Cu-2-4	215	15,417	1	167.3	169	-	-	0.78	0.26	-	-	14.5	2.3
Cu-2-6	225	685	1	175.1	178	3.166	0.96	0.49	0.29	83.2	24.8	16	2.5
Cu-2-5	230	565	1	179.0	178	-	-	0.96	0.30	-	-	18	2.7
Cu-5-1	170	16,107	–1	128.0	125	0.013	0.013	0.28	0.11	2.99	3.12	2.5	0.7
Cu-5-2	180	11,949	–1	135.6	135	0.091	0.069	0.3	0.13	1.81	1.59	3.1	0.9
Cu-5-3	200	13,550	–1	150.6	150	0.117	0.164	0.36	0.18	5.33	5.63	5.4	1.2
Cu-5-4	215	9,701	–1	161.9	165	-	-	0.36	0.22	-	-	7.5	1.6
Cu-5-5	230	3,953	0	173.2	175	-	-	1.1	0.26	-	-	13	1.9
Cu-5-6	245	20	1	184.5	185	2.64	0.632	0.87	0.30	79.8	18.7	10.5	2.2
Cu-18-1	230	3,952	0	165.6	165	-	-	0.84	0.24	-	-	6	1.5
Cu-18-2	240	3,331	0	172.8	175	-	-	1.29	0.26	-	-	8	1.7
Cu-18-3	255	147.5	1	183.6	182	2.527	1.039	1.51	0.31	78	30.8	9	2.1

k_R = –1 interrupted, k_R = 0 running, k_R = 1 ruptured

5 Discussion

5.1 Creep strain and notch deformation

Due to difficulty in measuring axial strain just within the notch during creep test and non-uniform deformation over the notch and the specimen, the overall axial strain measured within the gauge length of 51 mm is used to present behaviour of deformation versus time, see Figures 3-6. The local strain in the notch is of course much larger than average overall strain. The significance of Figures 3-6 is however to show the primary, secondary and tertiary creep in relation to stress and notch acuity.

The local deformation at rupture within notches is measured and the results in terms of local axial strain ε_a and local radial strain ε_r are given in Table 3-2. As expected, significant deformation takes place within the notches, e.g. the ratio between ε_a and the overall axial strain can be as high as 200 for the sharpest notch (a/R = 18.8) at 255 MPa. Comparing to the unbroken notch, both ε_a and ε_r are several times larger on the failed notch, see also Table 3-2. This implies that the notches may deform unevenly.

Unequal deformation on two notches can also be verified by measuring ε_a and ε_r for the interrupted tests, see Table 3-3. The fact that obvious differences in ε_a and ε_r between two notches are found on the failed tests indicates that considerable deformation occurs on smaller notches at later stages of creep test.

Linear relation between ε_a and ε_r, see Figure 3-7, makes it possible to estimate ε_r if ε_a is known, or vice versa. It is also noted that the relation is notch acuity dependent. The sharper the notch, the faster the ε_a increases.

5.2 Notch insensitivity/strengthening

An important result in the present investigation has been that the tested Cu-OFP material is insensitive to notches at 75°C, see Figure 3-5. This is the case for all the studied notch acuities. In fact, the creep lifetime under multiaxial stress state is longer than that under uniaxial stress state, indicating notch strengthening. The notch strengthening factor in time is greater than 70 at the net section stress of 180 MPa for the bluntest notch (a/R = 0.5). If the lifetimes are compared at given reference stresses the uniaxial and the multiaxial results are similar. This is in agreement with results for the same type of creep tests for 9 Cr1Mo steel /16/.

Notch strengthening has been observed in some other studies /17/–/19/. In /17/, the creep notch sensitivity by using round notched bar specimens with a/R = 13.3 has been investigated for a low alloy steel ASTM A508 and a cold worked microalloyed 0.15 C1.2Mn steel at 360°C. Both steels show a pronounced notch strengthening effect and the effect is somewhat stronger for the ASTM A508 than for the cold worked microalloyed steel. For another low alloy steel (BS 1501-271) /19/, round notched bar specimens with a/R = 15 were taken from as-received material and simulated coarse grained heat affected zone (SCGHAZ) across a weldment. The creep test results at 360°C exhibited a considerable notch strengthening. Post test metallography showed that for the notched tests carried on the SCGHAZ, transgranular and intergranular crack initiation and growth dominate at shorter and longer failure time, respectively.

Notch strengthening may be affected by ductility. The studied Cu-OFP is very ductile. Under uniaxial stress state, the creep strain at failure is around 50% /7/. Even higher strain has been locally obtained under multiaxial stress state, see Tables 3-2 and 3-3 as well as Figure 3-7. Considerable plastic deformation will change notch dimension, or notch acuity, which in turn alters the stress state. Actually, notch dimension/acuity starts to change from uploading. Overall axial strain at full load measured within the nominal gauge length of 51 mm as a function of net section stress for all the notch acuities is exhibited in Figure 5-1. Apparently, the overall axial strain at full load increases with increasing net section stress. At net section stresses greater than 180 MPa, the overall axial strain at full load exceeds in most cases 0.5%, implying occurrence of plastic deformation. Supposing the local axial strain within the notch is much larger than the overall one, cf Figures 3-6 and 9, notch dimension/acuity, and thereby stress state and stress concentration factor, may have been altered at full load, as the creep test begins.

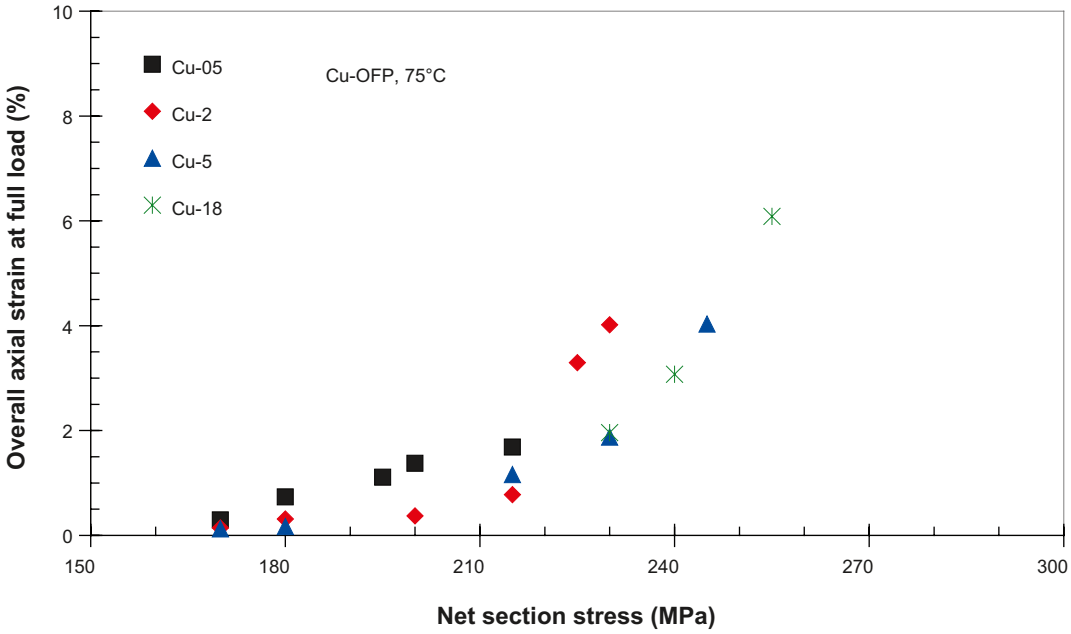

Figure 5-1. *Overall axial strain at full load as a function of net section stress for all the notch acuities.*

The numerical simulations could represent the behaviour well and also provided explanations to the notch strengthening.

In the creep investigation, the net section stress gives quite a conservative estimate of the lifetime if compared with a uniaxial creep rupture curve. But this result can still be used in design to give a first estimate of safety when a crack is present. A more accurate estimate is obtained if elastic plastic FEM-modelling is performed for a perfect plastic material. The resulting reference stress can be compared to the uniaxial creep rupture data. This estimate is not fully conservative. Some of the rupture stresses are found up to 5% below the uniaxial rupture line. A still more accurate approach is to include creep in the FEM-model. A prerequisite is that precise constitutive equations are available. For the investigated creep specimens the largest creep stresses can be found in a homogenous band around the notches. In this case the maximum stationary creep stresses are close to the reference stress, and the same conclusions about conservatism apply. However, if the creep stresses are varying across a component the results can be quite different in comparison to elasto-plastic analysis. The area with the largest stresses should be considered in design. These largest stresses should not exceed the uniaxial design stress.

5.3 Stress state

The significant stress parameters in the multiaxial stress rupture criterion (MSRC) /20/ have been considered to be: the maximum principal stress, σ_1, and the von Mises effective stress, σ_e, where stress directs intergranular creep damage dominates; the mean or hydrostatic stress, σ_m, and σ_e where continuum hole growth is the dominant fracture mechanism. The creep cavitation investigation on unbroken notch of failed specimens has shown that cavities are mainly found on the grain boundaries, see Figures 3-9b, 3-9c, 3-10b, 3-11b, and 3-12b. Due to the presence of very few cavities it is likely that the rupture is controlled by ductile processes.

Assuming that the MSRC is determined by both σ_1 and σ_e, then, the rupture life under multiaxial stress state, has traditionally been expressed by a mixed parameter control in the following two frequently used ways /21/–/24/:

$$t_{MR} = \frac{C(T)}{[\alpha \cdot \sigma_1 + (1-\alpha)\sigma_e]^{\nu_U}} \qquad \text{(Eq. 5-1)}$$

and

$$t_{MR} = \frac{C(T)}{\sigma_1^{\gamma} \cdot \sigma_e^{\nu_U - \gamma}} \qquad \text{(Eq. 5-2)}$$

where $C(T)$ is a function of temperature, ν_U the stress exponent under uniaxial stress state, α and γ are failure mechanism control parameters. Equation 5-1 is proposed by Sdobyrev /21/ and the constant α usually has a value close to 0.5. Equation 5-2 has been demonstrated in some studies /22/–/24/. γ is a significant parameter controlling the MSRC and it lies in the range $0 < \gamma < \nu_U$.

Equations 5-1 and 5-2 are only of interest in the present context if the introduction of fitting parameters can be avoided. For Equation 5-1 this is possible if $C(T)$ and ν_U are assumed to be given by the uniaxial data and that α takes the value 0.5. For Equation 5-2 this is not possible because γ is an arbitrary parameter. Thus, we disregard Equation 5-2.

It would be tempting to use Equation 5-1 to the data for the specimens with waist deformation in Figure 4-7, since Equation 5-1 would raise the values. Unfortunately, the equation strongly overcompensates the effect and cannot be applied to Cu-OFP.

Extended from plastic deformation of perfectly plastic materials, Bridgman /25/ gave an analytical solution of the von Mises effective stress σ_e across the notch throat in the steady state creep as below:

$$\sigma_e = \frac{\sigma_{net}}{(1 + \frac{2R}{a}) \cdot \ln(1 + \frac{a}{2R})} \qquad \text{(Eq. 5-3)}$$

It is of interest to check if Equation 5-3 gives reasonable values for the present tests. This is illustrated in Figure 5-2.

As can be seen from Figure 5-2, Equation 5-3 gives the right order of magnitude for stress ratio σ_{net}/σ_e for specimens with the lowest acuities 0.5 and 2, but gives too high values at the higher acuities. Obviously, Equation 5-3 is not applicable in the present case.

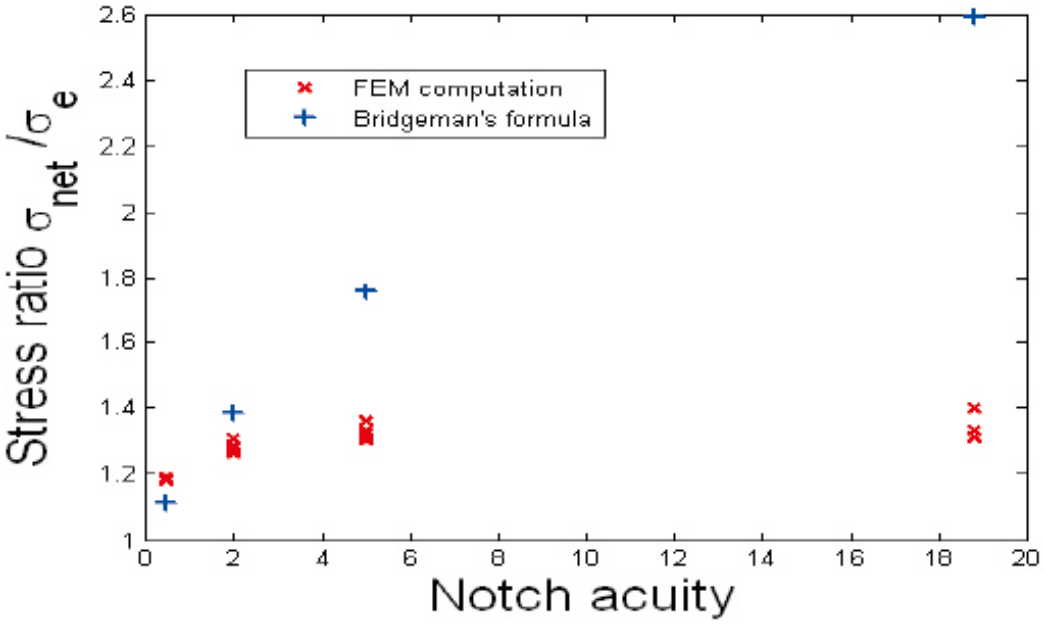

Figure 5-2. *Comparison of Bridgeman's formula (Eq. 5-3) to results of the FEM analysis.*

6 Recommendation for future work

The present investigation has demonstrated that the creep tested Cu-OFP material is not susceptible to notches at 75°C, possibly due to sufficient ductility which allows adaption of notch dimension/ acuity during creep. It should be noticed that the tested material is in as-hot worked soft condition, or annealed condition.

A recent study reports that cold work in both tension and compression in the same material as the present one reduces creep ductility considerably at 75°C, i.e. from 40% to 10% /26/. The reduced creep ductility may affect notch susceptibility and creep behaviour under multiaxial stress state. In fact, geometrical changes including notches are frequently associated with cold work caused by manufacturing and machining processes.

It is therefore recommended to study the effect of multiaxial stresses on creep properties of cold worked Cu-OFP.

7 Conclusions

The influence of multiaxial stresses on creep properties of Cu-OFP at 75°C has been studied by using double notch specimens with notch acuities of 0.5, 2, 5, and 18.8, respectively. The following conclusions can be drawn

1. The investigated Cu-OFP is insensitive to notch at 75°C. Actually, the creep lifetime under multi-axial stress state is longer than that under uniaxial stress state, indicating notch strengthening at the given net section stresses. The notch strengthening factor in time is, for instance, greater than 70 at 180 MPa for the bluntest notch ($a/R = 0.5$).
2. The sharper the notch, the longer the creep lifetime at the given net section stresses. At higher net section stresses, the sharpest notch ($a/R = 18.8$) has a lifetime about 10^4 times longer than the bluntest notch ($a/R = 0.5$) does.
3. The local deformation within the notch is measured and evaluated. Significant deformation takes place within the notch, *e.g*. the ratio between local axial strain within notch and overall axial strain within gauge length can be as high as 200, implying a strong underestimation of local deformation by the overall axial strain.
4. Unequal deformation on the two notches is observed. Both axial and radial strains on the failed notch are several times larger than those on the unbroken one. Linear relation between the axial and the radial strains on the notch is found.
5. Transgranular failure is predominant, independent of stress, rupture time, and notch acuity. Adjacent to fracture, elongated grains along the stress direction, few separate pores and cavities are often visible. On the unbroken notch, fewer separate cavities have been observed in several cases. In one specimen exposed to long term testing an intergranular crack was observed, probably as a result of linking of individual cavities. The observed metallography is consistent with the high creep ductility of Cu-OFP also under multiaxial stress states.
6. Using a fundamental creep model without fitting parameters, it has been possible to represent the creep strain curves for the notched specimens quite well. This is the case in spite of the very large difference in lifetime in comparison to uniaxial specimens at given net section stresses.
7. In the FEM-modelling of the creep deformation a stationary stress state was soon obtained. The highest stresses appeared in a band of constant stress around the notch. This constant stationary creep stress is close to the reference stress. For the blunter notch this band was at the centre of the notches, whereas for the sharper notch the band had a spherical form. In the band a main part of the creep deformation takes place.
8. Net-section stress can safely be used in design by verifying that it does not exceed the design stress. This gives, however quite a conservative estimate of the lifetime. A more accurate estimate is obtained if the elasto-plastic reference stress is used. A still more accurate procedure is to determine the stationary creep stress using FEM-modelling. In the case of a component where the creep stresses vary across it, the use of the maximum stationary creep stress is the best way of estimating the lifetime.
9. If the stationary stress was used the stress versus rupture times approximately fell on the same rupture curve as for the uniaxial data. In this way the rupture time of components can be predicted.

Acknowledgement

This work has been performed at KTH and Swerea KIMAB. The financial support from the Swedish Nuclear Fuel and Waste Management Co (SKB) is greatly acknowledged. The SKB is also thanked for providing the test material.

References

/1/ **Dyson B F, Loveday M S, 1981.** "Creep fracture in Nimonic 80A under triaxial tensile stressing", Proc. Creep in Structures, TUTAM Symp. Pergamon Press, Oxford, pp 406–421.

/2/ **Loveday M S, Dyson B F, 1979.** "Creep deformation and cavitation damage in Nimonic 80A under triaxial tensile stressing", Proc. ICM 3, Vol. 2, Cambridge, pp 213–222.

/3/ **Hayhurst D R, Webster G A, 1986.** "An overview on studies of stress state effects during creep of circumferentially notched bars", Techniques for multiaxial creep testing, edited by Gooch D J and How I M, Elsevier Applied Science, Chapter 9, pp 137–143.

/4/ **Hayhurst D R, Henderson J T, 1977.** "Creep stress redistribution in notched bars", International Journal of Mechanical Sciences, 19, pp 133–146.

/5/ **Webster G A, Aplin P F, Cane B J, Dyson B F, Loveday M S, 1992.** "A code of practice for notched car creep rupture testing: procedures and interpretations of data for design", Harmonisation of Testing Practice for High Temperature Materials, eds Loveday M S, Gibbons T B, Elsevier Applied Science, London, pp 295–330.

/6/ **Al-Faddagh K, Webster G A, Dyson B F, 1984.** "The influence of stress on the creep failure of 2¼Cr, 1Mo steel", Mechanical Behaviour of Materials IV, edited by Carlsson J, Ohlsson N G, Oxford, pp 289–295.

/7/ **Andersson H C M, Seitisleam F, Sandström R, 2007.** "Creep testing and creep loading experiments on friction stir welds in copper at 75°C", TR-07-08, Svensk Kärnbränslehantering AB.

/8/ **SKB 2006.** "Kapsel för använt kärnbränsle: Tillverkning av kapselkomponenter", R-06-03 Svensk Kärnbränslehantering AB, in Swedish.

/9/ **Jin L-Z, Sandström R, 2008.** Creep of copper canisters in power-law breakdown, Computational Materials Science, 43, pp 403–416.

/10/ **Jin L-Z, Sandström R.** Non-stationary creep simulation with a modified Armstrong-Frederick relation applied to copper canisters, to be published in Computational Materials Science.

/11/ **Jin L-Z, Sandström R, 2009.** "Modified Armstrong-Frederick relation for handling back stresses in FEM computations", Proceedings 2nd international ECCC conference. Creep & fracture in high temperature components – design & life assessment issues, Dübendorf, Switzerland, eds I A Shibli, S R Holdworth, 2009, pp 836–847.

/12/ **Sandström R, Andersson H C M, 2008.** "Creep in phosphorus alloyed copper during power-law breakdown", Journal of Nuclear Materials 372, pp 76–88.

/13/ **Sandström R, Andersson H C M, 2007.** "Creep during power-law breakdown in phosphorus alloyed copper", CREEP8 Conference, San Antonio, Texas, USA, July 22–26, 2007.

/14/ **Sandström R, Hallgren J, Burman G, 2009.** "Stress strain flow curves for Cu-OFP", R 09-14, Svensk Kärnbränslehantering AB.

/15/ **Andersson-Östling H C M, Sandström R, 2009.** Survey of creep properties of copper intended for nuclear waste disposal. SKB TR-09-32, Svensk Kärnbränslehantering AB.

/16/ **Takahashi Y, 2009.** Effect on creep damage by a combination of experiments and numerical analyses, ASME Pressure Vessels and Piping Division Conference, Prague, 2009.

/17/ **Storesund J, Tada N, Sandström R, 1992.** "Notch sensitivity of creep failure below the limit temperature", Swedish Institute for Metals Research, Report IM-2961, December, 1992.

/18/ **Browne R J, Flewitt P E J, Lonsdale D, Shammas M, Soo J N, 1991.** "Multiaxial creep of fine grained 0.5 Cr-0.5 Mo-0.25 V and coarse grained 1 Cr-0.5 Mo steels", Materials Science and Technology, Vol. 7, August, pp 707–717.

/19/ **Wu R, Seitisleam F, Sandström R, 1999.** "Creep crack growth in a high strength low alloy steel at 360°C, Proc. Int. Conf. Creep and Fracture of Engineering Materials and Structures, Tsukuba city, Japan, 1–5 of November 1999, pp 139–146.

/20/ **Hayhurst D R, 1972.** "Creep rupture under multiaxial states of stress", Journal of Mechanics Physical Solids, 20, 1972, pp 381–390.

/21/ **Sdobyrev V P, 1958.** Izv. Akad. Nauk SSSR, Otd. Tekh. Nauk. Vol 4, 1958, p 92.

/22/ **Needham N G, Gladman T, 1980.** "The Effect of Stress-State on the Processes Controlling Creep Fracture in a 2.25%Cr1%Mo Steel, C 190/80", © I Mech E, 1980, pp 49–54.

/23/ **Cane B J, 1979.** "Creep cavitation and rupture in 2.25 Cr1 Mo steel under uniaxial and multiaxial stresses", Int. Conf. Mechanical Behaviour of Metals, Vol 2, Cambridge, Pergamon Press, 1979, p 173.

/24/ **Lonsdale D, Flewitt P E J, 1978.** Proc. 5th Conf Strength of Metals and Alloys, Aachen, Pergamon Press, p 245.

/25/ **Bridgman P W, 1952.** "Studies in large plastic flow and fracture", McGraw-Hill, New York.

/26/ **Martinsson Å, Andersson-Östling H C M, 2009.** The effect of cold work on the creep properties of copper, 33rd Int. Symposium "Scientific Basis for Nuclear Waste Management", MRS 09, St. Petersburg, Russia, 2009.